HHS Public Access

Author manuscript

*Cell Rep*. Author manuscript; available in PMC 2021 June 14.

Published in final edited form as:

*Cell Rep*. 2021 May 18; 35(7): 109122. doi:10.1016/j.celrep.2021.109122.

# Essential role of the endocytic site-associated protein Ecm25 in stress-induced cell elongation

**Xudong Duan**[#1,2,3], **Xi Chen**[#1], **Kangji Wang**[1], **Li Chen**[1], **Oliver Glomb**[4], **Nils Johnsson**[4], **Lin Feng**[2], **Xiao-Qiu Zhou**[2,*], **Erfei Bi**[1,6,*]

[1]Department of Cell and Developmental Biology, Perelman School of Medicine, University of Pennsylvania, Philadelphia, PA 19104-6058, USA

[2]Animal Nutrition Institute, Sichuan Agricultural University, Chengdu, 611130 Sichuan, China

[3]Chongqing Institute of Green and Intelligent Technology, Chinese Academy of Sciences, Chongqing 400714, China

[4]Institut für Molekulare Genetik und Zellbiologie, Universität Ulm, 89081 Ulm, Germany

[#] These authors contributed equally to this work.

## SUMMARY

How cells adopt a different morphology to cope with stress is not well understood. Here, we show that budding yeast Ecm25 associates with polarized endocytic sites and interacts with the polarity regulator Cdc42 and several late-stage endocytic proteins via distinct regions, including an actin filament-binding motif. Deletion of *ECM25* does not affect Cdc42 activity or cause any strong defects in fluid-phase and clathrin-mediated endocytosis but completely abolishes hydroxyurea-induced cell elongation. This phenotype is accompanied by depolarization of the spatiotemporally coupled exo-endocytosis in the bud cortex while maintaining the overall mother-bud polarity. These data suggest that Ecm25 provides an essential link between the polarization signal and the endocytic machinery to enable adaptive morphogenesis under stress conditions.

## Graphical Abstract



[*]Correspondence: zhouxq@sicau.edu.cn (X.-Q.Z.), ebi@pennmedicine.upenn.edu (E.B.).

[6]Lead contact

AUTHOR CONTRIBUTIONS

Conceptualization, E.B.; investigation, X.D., X.C., O.G., K.W., and L.C.; data analysis, X.D., X.C., E.B., O.G., K.W., and L.C.; writing – original draft, E.B., X.D., and X.C.; writing, review, editing, and discussion, E.B., X.D., X.C., L.F., X.-Q.Z., N.J., O.G., K.W., and L.C.; supervision, E.B. and X.-Q.Z.

DECLARATION OF INTERESTS

The authors declare no competing interests.

SUPPLEMENTAL INFORMATION

Supplemental information can be found online at https://doi.org/10.1016/j.celrep.2021.109122.

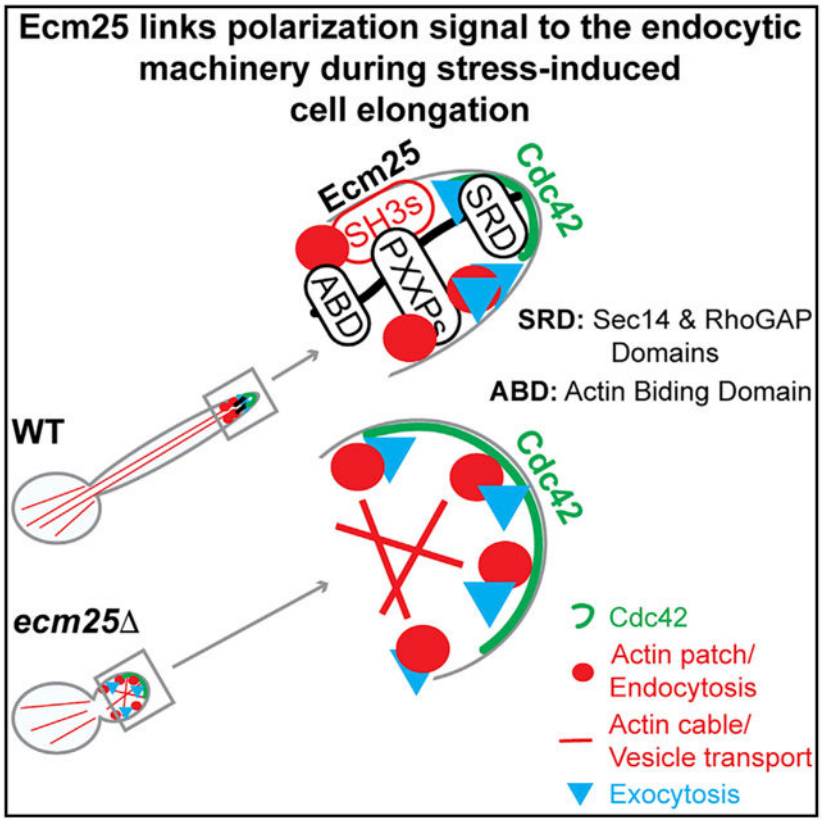


## In brief

How cells adopt a different morphology to cope with stress is not well understood. Duan et al. report that the budding yeast protein Ecm25 plays an essential role in stress-induced cell elongation by linking the polarity regulator Cdc42 to the late-stage endocytic machinery.

## INTRODUCTION

Each cell type has evolved a cell shape that best serves its function. The shaping mechanisms have been studied mainly in the context of polarized exocytosis in different cell types, including neurons (Nirschl et al., 2017), migrating animal cells (Sittewelle and Monsoro-Burq, 2018; Wesseling et al., 2018), pollen tubes in plants (Cai and Cresti, 2009; Onelli et al., 2015), and the budding yeast *Saccharomyces cerevisiae* (Bi and Park, 2012; Weiss, 2012). Because exocytosis and endocytosis are coordinated spatiotemporally in all eukaryotic cells (Battey et al., 1999; Gao et al., 2003; Grebnev et al., 2017; Gundelfinger et al., 2003; Johansen et al., 2016; Jose et al., 2013; Marco et al., 2007; Wu et al., 2014), it is possible that endocytosis could play an active role in cell shape determination by affecting exocytosis. Indeed, experimental and modeling studies suggest that localized endocytosis can modulate cell shape by recycling polarity regulators and exocytic components to sites of polarized cell growth (Caballero-Lima et al., 2013; Jose et al., 2013; Knafler et al., 2019; Marco et al., 2007; Shaw et al., 2011).

Cell shape can change profoundly in response to environmental stress. For example, *S. cerevisiae* undergoes sustained polarized growth to generate an elongated bud in response to nitrogen starvation (Gimeno et al., 1992) or treatment with hydroxyurea (HU) (Jiang and Kang, 2003; Kang and Jiang, 2005) or short-chain alcohols (Dickinson, 1996; Lorenz et al., 2000). These elongated cells form chains to allow cells to forage for food over a long distance (Gimeno et al., 1992; Kang and Jiang, 2005). Such a morphogenetic change is thought to be beneficial for cell survival under stress conditions. However, it is unclear how the exo-endocytic machinery is regulated under such conditions to enable cell shape change.

How polarized exocytosis in *S. cerevisiae* drives formation of an ovoid bud is largely understood at the molecular level. Polarized cell growth is initiated by activation and polarization of Cdc42 at the presumptive bud site (Adams et al., 1990; Okada et al., 2013; Ziman et al., 1993). Cdc42 is activated by its guanine nucleotide exchange factor (GEF) Cdc24 and inactivated by its GTPase-activating proteins (GAPs) (Park and Bi, 2007; Zheng et al., 1994). After bud emergence, polarized Cdc42 directs exocytosis toward the bud tip or “apical” site to drive bud elongation. Upon entry into mitosis, Cdc42 is distributed randomly along the bud cortex to drive “isotropic” growth of the bud while the overall mother-bud polarity is maintained. Such a cell cycle-controlled switch from apical to isotropic growth leads to generation of an ovoid bud (Lew and Reed, 1993). Importantly, conditional loss of Cdc42 activity completely blocks the “polarization” of exocytosis without blocking exocytosis per se (Adams et al., 1990; Sloat et al., 1981; Zhang et al., 2001). Thus, it is the directionality, not the activity, of exocytosis that dictates cell shape. Actin patches (i.e., the endocytic sites) are also polarized in a Cdc42-dependent manner (Adams et al., 1990). The endocytic sites are assembled and matured progressively with early-arriving proteins involved in coat assembly and cargo uptake and late-arriving proteins involved in Arp2/3-nucleated actin polymerization and subsequent actin-dependent membrane invagination and fission (Carroll et al., 2012; Goode et al., 2015; Kaksonen et al., 2003, 2005). How Cdc42 controls the polarization of endocytosis remains poorly understood. It is also unclear whether spatial control of endocytosis could dictate a morphogenetic outcome, as in the case of exocytosis.

*ECM25* (extracellular mutant 25) in *S. cerevisiae* was first identified in a genetic screen for mutants that are hypersensitive to Calcofluor White, a fluorescent dye that binds to chitin and, to a lesser degree, glucan, and interferes with their assembly into microfibrils (Lussier et al., 1997). Further analysis did not reveal any specific defects in cell wall synthesis in *ecm25* mutants (Lussier et al., 1997). *ECM25* was also identified in a genetic screen for mutants that are deficient in stress-induced filamentous growth (Kang and Jiang, 2005). In this study, we demonstrate that Ecm25 associates with late-stage endocytic sites and interacts with Cdc42, several endocytic proteins, and F-actin. Deletion of *ECM25* does not affect cell growth or cell shape under normal growth conditions but, remarkably, abolishes HU-induced cell elongation, which is accompanied by depolarization of endocytosis and exocytosis. These observations suggest that, under stress conditions, Ecm25 links the Cdc42-based polarization signal to the endocytic machinery, which, in turn, modulates exocytosis to control cell morphogenesis.

# RESULTS

## Ecm25 is essential for stress-induced cell elongation

A genetic screen implicated Ecm25 in stress-induced filamentous growth (Kang and Jiang, 2005). However, no further studies have been carried out to define its function and mechanism. Ecm25 contains a cryptic CRAL/TRIO/Sec14-like domain that binds to several lipids (Gallego et al., 2010; Panagabko et al., 2003), a RhoGAP domain with apparent absence of the catalytic “arginine finger” (Ahmadian et al., 1997; Rittinger et al., 1997), and three PXXP motifs that are generic binding sites for SH3 domains (Feller et al., 1994; Figure 1A). To define its functions, we first deleted *ECM25* in the yeast strain BY4741 (Brachmann et al., 1998). The deletion did not cause any obvious defects in cell growth (Figure S1A), cell morphology (Figures 1B and 1C), and cell cycle progression (Figures S1B and S1C; Video S1). Consistent with a previous report (Kang and Jiang, 2005), a sub-lethal dosage of HU (100 mM) caused wild-type (WT) cells to form elongated buds at 25°C (Figures 1B and 1C). Remarkably, this phenotype was abolished by deletion of *ECM25*. In addition, *ecm25Δ* cells failed to form colonies on plates containing 200 mM HU at 30°C (Figure 1D). Thus, Ecm25 is required not only for HU-induced cell elongation at 25°C but also for cell survival at 30°C under HU-imposed cell stress.

Environmental stress is known to trigger filamentous growth or bud elongation through a G2 delay caused by Swe1 kinase-mediated inhibition of CDK1 (Cdc28)/mitotic cyclin (Clb2) activity (Keaton and Lew, 2006; Rua et al., 2001). We found that deletion of *SWE1* caused a small but significant defect in HU-induced cell elongation (Figures 1B and 1C; Wu and Jiang, 2005). Strikingly, the length/width ratios of the buds for *swe1Δ ecm25Δ* cells were nearly identical to those of *ecm25Δ* cells in the presence of HU (Figures 1B and 1C), suggesting that Ecm25 acts downstream of Swe1. This conclusion is further supported by the observation that deletion of *ECM25* did not cause any obvious defects in cell cycle progression (Figures 1E and 1F; Video S1). Thus, Ecm25 plays an essential role in HU-induced cell elongation downstream of Swe1-mediated cell cycle control.

Deletion of the DNA damage checkpoint and DNA replication checkpoint kinase Rad53 is known to cause Swe1-dependent cell elongation (Enserink et al., 2006; Pardo et al., 2017), which can be enhanced by HU treatment (Enserink et al., 2006). This was confirmed in our experiment (Figures 1B and 1C). Remarkably, the elongated bud morphology of *rad53Δ* cells in the presence or absence of HU was nearly abolished by *ecm25Δ* (Figures 1B and 1C). This observation suggests that Ecm25 plays an essential role in *rad53Δ*-induced cell elongation.

We also performed similar experiments in the YEF473 background (Bi and Pringle, 1996) and obtained qualitatively similar results (Figures S1D and S1E). In this background, 100 mM HU also induced elongated bud morphology but to a lesser degree than in the BY background. This elongated bud morphology was abolished by *ecm25Δ* but not *swe1Δ*. As reported in other strain backgrounds, deletion of the septin subunit Shs1 in the YEF background caused Swe1-dependent bud elongation (Carroll et al., 1998; Egelhofer et al., 2008; Mino et al., 1998), which was enhanced by HU treatment (Smolka et al., 2006). Similar to *rad53Δ* cells, the elongated bud morphology of *shs1Δ* cells in the presence or

absence of HU was also abolished by *ecm25Δ*. Thus, the requirement of Ecm25 for HU- or mutationally induced cell elongation is independent of strain background (all experiments described hereafter were performed in the BY strain background).

These data suggest that Ecm25 plays an essential role in cell elongation induced by various stresses through a mechanism that functions downstream of cell cycle control.

## Ecm25 is required for sustained polarization of exo-endocytosis at the bud tip during stress-induced cell elongation

In *S. cerevisiae*, polarized cell growth is driven by polarized exocytosis (Bi and Park, 2012; Zeng et al., 2017). To determine how Ecm25 might function in cell elongation, a form of sustained polarized cell growth, we first monitored exocytosis in HU-treated WT and *ecm25Δ* cells throughout the cell cycle by following the post-Golgi vesicle-associated exocyst subunit Exo84 (Boyd et al., 2004; Guo et al., 1999a). Surprisingly, exocytosis was sustained near the bud tip in WT cells even during the G2/M phases (Figures 2A and 2B; Video S2), when non-treated cells are known to undergo isotropic bud growth (Lew and Reed, 1993). In contrast, exocytosis was no longer targeted toward the bud tip during the same cell cycle stages in *ecm25Δ* cells (Figures 2A and 2C; Video S2). The duration of Exo84 at the bud tip was longer in WT cells than in *ecm25Δ* cells (Figure 2D). Similar results were obtained with another exocytic marker, the Rab GTPase Sec4 (Figures S2A–S2D; Video S3), which is required for transport of post-Golgi vesicles from the mother cell compartment to the bud as well as for tethering the vesicles to the plasma membrane (PM) (Guo et al., 1999b; Salminen and Novick, 1987). These data indicate that Ecm25 is required for polarization of exocytosis at the bud tip in HU-treated cells.

Because exocytosis and endocytosis are known to be coupled spatiotemporally during polarized cell growth in all eukaryotes, including the budding yeast *S. cerevisiae* (Battey et al., 1999; Gao et al., 2003; Gundelfinger et al., 2003; Johansen et al., 2016; Jose et al., 2013), we also monitored endocytosis, together with exocytosis, in HU-treated WT and *ecm25Δ* cells using the exocytic marker Exo84-GFP and the endocytic marker Abp1-RFP (Kaksonen et al., 2003). In WT cells, both processes were directed toward the bud tip to drive cell elongation for an extended period of time (Figures 2E–2G and 2J; Video S2). In contrast, both processes were quickly depolarized from the bud tip toward the bud cortex in *ecm25Δ* cells while maintaining the overall mother-daughter polarity (Figures 2E and 2H–2J; Video S2). Thus, Ecm25 is required for sustained polarization of exocytosis and endocytosis toward the bud tip in HU-treated cells.

## The association of Ecm25 with endocytic sites is critical for its role in stress-induced cell elongation

Because exocytosis and endocytosis are linked spatiotemporally, it remained unclear whether Ecm25 controls HU-induced cell elongation primarily via exocytosis or endocytosis or both. To distinguish these possibilities, we first analyzed localization of endogenous Ecm25 during the cell cycle in HU-treated or untreated cells. In the absence of HU, Ecm25-GFP localized to Abp1-RFP-marked actin patches at sites of polarized cell growth (Figure 3A). Both proteins appeared to localize to and disappear from the cortical patches at about

the same time (Figures 3B, 3C, S3A, S3B, S3D, and S3E), with Ecm25 peaking slightly before Abp1 at the patch (Figures 3D, S3C, and S3F). The localization patterns and accumulation kinetics of Ecm25 and Abp1 in the presence of HU were similar to those observed in the absence of stress, with the exception that their duration at the patch was increased (Figures 3E–3G and S3G–S3L). Abp1 binds to the Arp2/3-nucleated actin filaments and is a marker of late-stage endocytic patches (Kaksonen et al., 2003, 2005; Young et al., 2004). These data indicate that the endogenous Ecm25 associates with late-stage endocytic sites.

To determine whether the patch association of Ecm25 is important for its function, we targeted endogenous Ecm25 to or away from actin patches using the GFP-nanobody/binding peptide (GBP) system (Kubala et al., 2010; Rothbauer et al., 2006) and then monitored the effect on HU-induced cell elongation. The GFP-tagged actin patch component Sla1 and the GFP-tagged ATP-binding cassette (ABC) transporter Pdr5, which is known to localize predominantly to the mother side of the PM (Yang et al., 2015), were chosen as localization drivers. Because Sla1 and Pdr5 are more abundant than Ecm25, and because the affinity for GFP-GBP interaction is rather high (Kubala et al., 2010; Rothbauer et al., 2006; Tkach et al., 2012), GFP-tagged Sla1 and Pdr5 should be ideal localization drivers to target Ecm25-mApple-GBP to the desired cellular locations. As expected, targeting Ecm25 to actin patches by Sla1, which presumably adds an interaction between Ecm25 and endocytic sites via GFP-GBP, did not affect HU-induced cell elongation compared with WT cells (Figures 3H and 3J). In stark contrast, targeting Ecm25-mApple-GBP via Pdr5-GFP to the PM of the mother cell reduced HU-induced cell elongation to the level displayed by *ecm25Δ* cells (Figures 3I and 3J). As expected, when Ecm25 was not tagged with GBP, Pdr5-GFP did not affect HU-induced cell elongation or enrichment of Abp1-mRuby3 at the bud tip (Figure 3K). These data suggest that the association of Ecm25 with actin patches is essential for its function and that Ecm25 likely controls endocytosis to drive HU-induced cell elongation.

## The N-terminal Sec14-like and RhoGAP domains of Ecm25 mediate its interaction with Cdc42 and are required for stress-induced cell elongation

How does Ecm25 associate with the polarized actin patches during bud growth? The facts that Ecm25 contains a RhoGAP domain, which is known to mediate interactions between Rho-GAPs and small GTPases (Amin et al., 2016; Gladfelter et al., 2002; Li et al., 1997), and that Cdc42 is also required for HU-induced cell elongation (Wu and Jiang, 2005) raise the possibility that Ecm25 may provide a link between Cdc42 and the actin patches. To test this possibility, we first examined the interactions between Cdc42 and different Ecm25 fragments using the bimolecular fluorescence complementation (BiFC) assay (Hu et al., 2002; Sung and Huh, 2007). Full-length Ecm25 displayed no apparent interaction with Cdc42 at sites of polarized growth, but the N-term+RhoGAP fragment displayed a clear and consistent interaction (Figure 4A). In contrast, N-term alone, RhoGAP alone, and C-term did not interact at all (Figure 4A). As expected, none of the negative controls, including the strains expressing the C-terminal fragment of Venus (VC)-Cdc42 only, VC-Cdc42 and the N-terminal fragment of Venus (VN) expressed from the *ECM25* promoter (i.e., *Pecm25*-VN), or Ecm25-VN only (i.e., full-length [FL]-VN), showed any BiFC signal (Figure 4A). Thus, the Sec14-like and the RhoGAP domains together are capable of interacting with

Cdc42 at sites of polarized cell growth. None of the measured interactions were influenced by the presence of HU in the culture medium.

We next purified FL Ecm25 and its fragments as maltose-binding protein (MBP) fusions and examined their interactions with glutathione S-transferase (GST) fusions of the WT, the mutationally locked GTP-bound form (Q61L), or the GDP-bound form (T17N) of Cdc42 (Figure S4A). As expected, the positive control MBP-Gic2, a well-characterized effector of Cdc42 (Brown et al., 1997; Chen et al., 1997; Okada et al., 2017), interacted strongly and specifically with Cdc42-Q61L, whereas the negative control MBP did not interact with any form of Cdc42 or GST alone. Under the same conditions, the FL and the RhoGAP domain of Ecm25 displayed very weak (barely above the background) interactions with all three forms of Cdc42, whereas the N-term and C-term of Ecm25 did not interact at all with any forms of Cdc42. Consistent with the BiFC data, only the N-term+RhoGAP fragment interacted clearly with all three forms of Cdc42 (Figure S4A). Because Ecm25 does not interact specifically with GTP-bound Cdc42, it is not considered a *bona fide* effector of Cdc42. This feature is not unique to Ecm25. Other important regulators of Cdc42, such as the armadillo repeat-containing protein Bem4 (Mack et al., 1996; Pitoniak et al., 2015) and the Rho GDP-dissociation inhibitor (RhoGDI) Rdi1 (Johnson et al., 2009; Logan et al., 2011) also bind to Cdc42 in a nucleotide state-independent manner. The BiFC and the *in vitro* binding data suggest that Ecm25 interacts with Cdc42 via its N-terminal Sec14-like and RhoGAP domains.

What is the function of the Ecm25-Cdc42 interaction? Ideally, this question should be addressed by identifying and characterizing mutations in *ECM25* that specifically disrupt its interaction with Cdc42. However, because a large region of Ecm25 (residues 1–360; Figure 1A) is involved in this interaction, it is difficult and very time-consuming to identify such mutations without a crystal structure of the complex. Nonetheless, we performed several alternative experiments to address this question. First, we found that Ecm25-GFP was depolarized when Cdc42 was conditionally inactivated at 37°C by a temperature-sensitive mutation in its GEF; i.e., *cdc24-4* (Figure S4B). This is consistent with the idea that Ecm25 serves as a linker between the upstream Cdc42 and the downstream actin patches. Second, we monitored Cdc42 activity in WT and *ecm25Δ* cells using Gic2PBD(W23A)-GFP, a biosensor for Cdc42-GTP (Okada et al., 2013, 2017). After HU treatment for 6 h, small- or large-budded WT and *ecm25Δ* cells displayed a similar localization profile and/or activity of Cdc42 (Figures S4C–S4E). Thus, Ecm25 does not appear to affect Cdc42 activity. This is consistent with Ecm25 being a “dead” GAP for Cdc42 because it lacks the catalytic “arginine finger” (Ahmadian et al., 1997; Rittinger et al., 1997); otherwise, Cdc42 activity would be expected to increase in *ecm25Δ* cells. It also suggests that Ecm25, if acting downstream of Cdc42, does not control Cdc42 activity via a feedback mechanism. These data, together with the observations of Ecm25 association with endocytic sites (Figure 3A) and of depolarized endocytosis in HU-treated *ecm25Δ* cells during bud growth (Figure 2E), suggest that Cdc42 might control polarized distribution of endocytosis via Ecm25 during HU-induced cell elongation.

Next we deleted the Cdc42-binding region or its subfragments in Ecm25 and then examined their effect on Ecm25 localization and function. We constructed a series of strains containing

*ecm25Δ*, *ABP1-RFP*, and a plasmid expressing a *MET25* promoter-controlled, N-terminal GFP tag fused to FL Ecm25 (residues 1–599) or different Ecm25 fragments. In the absence of HU, GFP expressed from the plasmid vector localized in the cytoplasm, whereas FL Ecm25 co-localized with Abp1 in actin patches (Figure 4B). In contrast, the Sec14 domain-containing N-term fragment (residues 1–189) or the RhoGAP domain (residues 190–360) of Ecm25 was mainly cytosolic and formed a few "puncta" that did not co-localize with Abp1 (Figure 4B). When these two domains were combined to form the Cdc42-binding site in Ecm25 (Figures 4A and S4A), the resulting fragment formed more and brighter puncta that were polarized toward the bud but still failed to co-localize with Abp1 (Figure 4B). Thus, the Cdc42-binding region is sufficient for Ecm25 polarization but not for its association with endocytic sites. Strikingly, the C-term fragment (residues 361–599) localized to patch- and cable-like structures (Figure 4B). These patch-like structures co-localized with Abp1 (Figure 4B), whereas the cable-like structures co-localized with actin cables, as revealed by phalloidin staining (Figure 4C). Both structures were sensitive to Latrunculin A (LatA) (Figure 4D), a drug that disrupts all actin filaments by sequestering actin monomers (Ayscough et al., 1997). Thus, the C-term of Ecm25 is capable of interacting with actin patches and actin cables. When the N-term or RhoGAP domain was combined with the C-term, the resulting fragments formed more puncta than cables in comparison with the C-term alone, and these puncta co-localized with Abp1 (Figure 4B). These data suggest that the Cdc42-binding region plays a role in promoting Ecm25 association with actin patches and/or preventing its association with actin cables. Regardless of the mechanism, this role does not depend on its ability to bind to Cdc42-GTP because Ecm25 was still associated exclusively with actin patches when Cdc42 was inactivated (Figure S4B).

To determine the role of Cdc42 binding in Ecm25 function, we constructed a series of strains containing *ecm25Δ* or an allele of *ECM25* at the physiological locus in which the coding sequence for a specific domain was removed precisely. These strains were treated with HU, and the bud length/width ratios were measured for each strain. As expected, the bud length/width ratio was significantly lower in *ecm25Δ* cells than in the WT (Figures 4E and 4F). However, the Cdc42-binding region or the C-term fragment alone completely failed to rescue the *ecm25Δ* phenotype (Figures 4E and 4F). Even smaller deletions within the Cdc42-binding site (e.g., deletion of the N-term only [RhoGAP+C-term] or deletion of the RhoGAP only [N-term+C-term]) still caused significant defects in HU-induced cell elongation despite the fact that the RhoGAP domain or the RhoGAP+C-term fragment was able to rescue the defect to some degree (Figures 4E and 4F). These data indicate that the Cdc42-binding region and the C-term fragment of Ecm25 are each necessary, but not sufficient, for its role in HU-induced cell elongation.

All non-functional fragments mislocalized in the cell. To separate location from function, we used Sla1-GFP to drive the FL or different fragments of Ecm25 tagged with mApple-GBP to the actin patches and then assessed their effect on HU-induced cell elongation. As expected, Ecm25 FL was fully functional in this assay (Figures 4G and 4H). In contrast, none of other fragments, including the N-term, N-term+RhoGAP, and Ecm25 lacking the Xudong's actin binding (xACT) motif (a newly identified F-actin-binding motif in the C-terminal region of Ecm25, so named in recognition of X.D.'s hard work in defining this region) were able to support HU-induced cell elongation (Figures 4G and 4H). Thus, the Cdc42-binding region,

even when directed to the actin patches, does not rescue the *ecm25Δ* phenotype. These data also indicate that xACT-mediated binding of Ecm25 to actin filaments at endocytic sites is essential for its role in HU-induced cell elongation.

These data indicate that the Cdc42-binding region of Ecm25 controls its polarized localization during the cell cycle, whereas its C-term is essential for its association with the actin patches. These data also indicate that each domain of Ecm25 is necessary, but not sufficient, for its essential role in HU-induced cell elongation.

## Ecm25 binds to actin filaments in budding yeast, fission yeast, and mammalian cells via an unexpected motif in its C-terminal region

The localization study suggests that Ecm25 might bind F-actin directly via its C-term. To test this possibility, we purified the FL and different fragments of Ecm25 as MBP fusions from bacteria and tested their abilities to bind F-actin using a standard pelleting assay (Figure 5A). As expected, a majority of actin was in the pellet for the “F-actin alone” sample (Figure 5A, lane 1). The positive control α-actinin was mainly in the supernatant in the absence of F-actin (lane 2) but was shifted to the pellet in the presence of F-actin (lane 3), whereas the negative control BSA largely remained in the supernatant even in the presence of F-actin (lane 4). Strikingly, MBP-Ecm25-FL (Figure 5A, lanes 5 and 6) and MBP-Ecm25-C-term (lanes 7 and 8) bound robustly to F-actin, whereas MBP-Ecm25-N-term +RhoGAP (lanes 9 and 10) did not bind at all. These data indicate that Ecm25 binds F-actin directly via its C-term.

Further structure-function analysis narrowed the F-actin-binding region in Ecm25 to a fragment spanning residues 536–588, which we designated xACT (Figure 5A). GFP-tagged xACT, but not its upstream sequence (amino acids [aa] 361–530), expressed from a heterologous promoter in budding yeast decorated mainly actin cables, and, to a lesser degree, actin patches (Figure 5B). In agreement, the bacterially expressed MBP-Ecm25-xACT bound to F-actin *in vitro* (Figure 5C). Strikingly, GFP-xACT expressed in fission yeast also labeled actin patches, actin cables, and the actin ring, and LatA treatment abolished all F-actin structures as well as GFP-xACT localization (Figure 5D). Similarly, GFP-xACT expressed in mammalian cells (HeLa-Kyoto cells) also labeled various F-actin structures (Figure 5E). LatA treatment disrupted these structures and GFP-xACT localization (Figure 5E). Even the remaining GFP-xACT signal displayed near-perfect co-localization with the remaining F-actin structures (Figure 5E). These data demonstrate that Ecm25 is capable of binding actin filaments in different organisms via an unexpected motif, xACT, in its C terminus.

## Ecm25 interacts with the SH3 domains of actin patch components via distinct PXXP motifs

The observation that FL Ecm25 localizes to actin patches but not cables (Figure 3A) and binds to F-actin via the xACT motif (Figure 5C) suggest that Ecm25 might also interact with other patch components to achieve its cellular selectivity for patches over cables. To test this possibility, we searched the *Saccharomyces* Genome Database (SGD) for candidate interactors of Ecm25. Three of the eight potential physical interactors identified from different high-throughput screens are patch components (Sla1, Lsb3, and Ysc84) and contain

at least one SH3 domain (Figure 6A). The other five proteins are involved in transcription and translation control (SGD). These proteins do not show any obvious connection to Ecm25 in terms of cellular localization and function and, thus, were not pursued further. Sla1 is thought to link clathrin coat formation to actin assembly during endocytosis because it is a clathrin adaptor (Tolsma et al., 2018) that binds to the Wiskott-Aldrich syndrome protein (WASP)-like protein Las17 (Drees et al., 2001; Gavin et al., 2006; Tonikian et al., 2009). Lsb3 and Ysc84 are paralogs that bind to Sla1 and Las17 (Dewar et al., 2002; Gavin et al., 2006; Madania et al., 1999; Tarassov et al., 2008; Tonikian et al., 2009) and are thought to regulate actin polymerization during endocytosis (Robertson et al., 2009). To confirm these potential interactions, we performed *in vitro* protein-binding assays using GST fusions of the candidate proteins (Sla1, Lsb3, and Ysc84) and MBP fusions of Ecm25 (FL and different fragments). The FL Sla1 (residues 1–1244) (data not shown) and its SH3 domain-containing N terminus (residues 1–420) (Figures 6A and 6B) bound to the FL Ecm25, whereas the C-terminal fragment of Sla1 (residues 418–1244) did not (data not shown). Because the GST fusions of the FL and C-terminal fragment of Sla1 were prone to degradation, they were not included for further analysis. As shown in Figure 6B, GST-Sla1(1–420aa), GST-Lsb3, and GST-Ysc84 interacted specifically with MBP-Ecm25-FL and MBP-Ecm25-C-term but not with any other Ecm25 fragments. Thus, the potential interactions between Ecm25 and Sla1, Lsb3, or Ysc84 have been confirmed, and, more importantly, direct binding between Ecm25-C-term and Sla1(1–420aa), Lsb3, or Ysc84 has been demonstrated.

Genome-wide two-hybrid analysis of the yeast SH3 domain interactome suggests that SH3 domains 1 and 2 but not 3 of Sla1 as well as the SH3 domains of Lsb3 and Ysc84 interact with the FL Ecm25 (Tonikian et al., 2009; Figure 6A). To confirm and extend this observation, we performed a series of *in vitro* protein binding assays. First, we found that mutations in the first and second SH3 domains (W41S and W108S, respectively) of GST-Sla1(1–420aa) (Tonikian et al., 2009) decreased its interaction with MBP-Ecm25-FL, MBP-Ecm25-C-term, and MBP-Ecm25(361–535aa) in a similar way, with the second SH3 domain playing a more prominent role (Figures 6A and 6C). In contrast, MBP-Ecm25(536–599aa) (slightly larger than xACT) failed to interact with any form of GST-Sla1(1–420aa) (Figures 6A and 6C). Thus, we defined a small region of Ecm25 (361–535aa) that directly binds to Sla1. Second, we found three potential PXXP-like motifs in Ecm25-C-term that might mediate its interactions with the SH3 domains of the patch components (Figure 6A). All three sites are mapped in the region of Ecm25 (361–535aa) that is engaged in the interaction with the SH3 domains of Sla1 (Figures 6A and 6C). Each of these PXXP motifs was mutagenized at both proline residues in the context of the MBP-Ecm25(361–535aa) fragment, resulting in three variants: MBP-Ecm25-m1, -m2, and -m3 (Figures 6A and 6D). These variants, together with the WT, were tested for interactions with GST fusions of Sla1(1–420aa), Lsb3, and Ysc84. Strikingly, the m1 and m2 variants displayed moderate but specific and consistent defects in their interactions with Sla1, Lsb3, and Ysc84, respectively (Figure 6D), suggesting that the first and second PXXP motifs of Ecm25 mediate its interactions with Sla1 and Lsb3/Ysc84, respectively (Figure 6A). These data, together with the previous two-hybrid analysis (Tonikian et al., 2009), indicate that Ecm25 interacts with the SH3 domains of Sla1, Lsb3, and Ysc84 via distinct PXXP motifs.

To determine the effect of the interactions between Ecm25 and the actin patch components on Ecm25 localization, we performed the following experiments. First, we found that the GFP-Ecm25-C-term patches co-localized with the patches of Sla1, Lsb3, and Ysc84 (Figure S5A). Second, the number of GFP-Ecm25-C-term patches was reduced significantly in the absence of Sla1, Lsb3, or Ysc84, with *sla1Δ* cells showing the most prominent effect (Figures S5B and S5C). Finally, GFP-Ecm25-C-term (361–599aa) formed far more patches than GFP-Ecm25-xACT (536–588aa) (Figures S5D and S5E). Collectively, these data suggest that the interactions of Ecm25 with the three patch components, especially Sla1, are important for its patch localization.

Surprisingly, GFP-Ecm25(361–530aa) (i.e., the N-terminal region of Ecm25-C-term that contains the binding sites for Sla1, Lsb3, and Ysc84; Figure 6A), localized to the cytoplasm and not to actin patches (Figure 5B), suggesting that these interactions alone are not sufficient to bring Ecm25 to the patches. In support of this conclusion, patch localization of endogenous Ecm25 was completely abolished by LatA treatment (Figure S5F), suggesting that even the FL Ecm25 cannot be recruited to or maintained at patches in the absence of its binding to actin filaments. These data suggest that Ecm25 localizes to endocytic patches via multi-valent interactions with Sla1, Ysc84, Lsb3, and F-actin.

Because the m1 and m2 mutations in the PXXP motifs of Ecm25 caused moderate but specific defects in its interactions with Sla1 and Lsb3/Ysc84, respectively (Figures 6A and 6D), we examined the effect of the combined mutations on Ecm25 localization and function. We constructed a strain in which the endogenous *ECM25* was replaced precisely with the *ecm25-m1m2* allele. Strikingly, the double mutations abolished HU-induced cell elongation (Figures S6A and S6B) despite the fact that the mutant protein was expressed at a level similar to the WT protein, as judged by western blotting (Figure S6C) or fluorescence microscopy (Figure S6D). The overall association of Ecm25-m1m2 with actin patches was decreased (Figure S6E), as indicated by the decrease in the percentage of actin patches (Abp1-mRuby3) harboring an Ecm25-m1m2-GFP signal versus a WT Ecm25-GFP signal (Figure S6F; Manders' M2 coefficient), whereas the percentages of green patches for WT Emc25-GFP and mutant Ecm25-m1m2-GFP harboring a red signal (Abp1-mRuby3) were unchanged (Figure S6F; Manders' M1 coefficient) (Manders et al., 1993). The decrease in association of Ecm25-m1m2 with actin patches was corroborated by its corresponding increase in the cytoplasm (Figure S6G). These data suggest that the interactions of Ecm25 with the actin-patch components are important for its localization and function.

## Ecm25 does not play a major role in fluid-phase and clathrin-mediated endocytosis

Because endogenous Ecm25 interacts with F-actin and other patch components via distinct motifs, we wanted to find out whether Ecm25 would affect actin patch behavior. Thus, we measured the number and lifespan of actin patches in WT and *ecm25Δ* cells in the presence or absence of HU. The numbers of actin patches in WT and *ecm25Δ* cells were comparable under the same growth condition (Figure 7A). The lifespans of actin patches in WT and *ecm25Δ* cells in the absence of HU were also comparable (Figure 7B). In the presence of HU, the lifespan of actin patches was lengthened significantly in WT but not in *ecm25Δ* cells (Figure 7B). In addition, the lifespan of actin patches in *ecm25Δ* cells was shortened

slightly but significantly compared with that in WT cells (Figure 7B).Except for a mild effect on actin patch lifespan in the presence of HU, deletion of *ECM25* does not overtly affect actin patch behavior.

To determine whether Ecm25 is required for endocytic function, we assessed fluid-phase and clathrin-mediated endocytosis in WT and different mutants by performing Lucifer Yellow (LY) staining (Tang et al., 2000; Wiederkehr et al., 2001) and analyzing the localization of Wsc1, a transmembrane cell wall stress sensor for a Rho1 signaling pathway and a well-defined endocytic cargo (Feliciano and Di Pietro, 2012), respectively. As expected, in the absence of HU, LY was internalized effectively and transported to the vacuole (the yeast equivalent of lysosomes in animal cells) in WT cells, and this process was compromised most severely in *sla1Δ* cells, moderately in *lsb3Δ* cells, and mildly in *ysc84Δ* cells (Figures 7C and 7D; Dewar et al., 2002; Gourlay et al., 2003). Not surprisingly, the *sla1Δ lsb3Δ ysc84Δ* triple mutant cells were even more defective in LY uptake than any of the single mutants (Figures 7C and 7D). Surprisingly, *ecm25Δ* cells showed only a mild defect in LY uptake (Figures 7C and 7D), despite its interactions with all three patch components. A similar pattern of LY uptake was observed in the same strains in the presence of HU. These data indicate that Ecm25 plays only a minor role in fluid-phase endocytosis.

Wsc1 contains an NPFxD endocytic internalization motif that binds to Sla1 during clathrin-mediated endocytosis (CME) (Ayscough et al., 1999; Feliciano and Di Pietro, 2012; Howard et al., 2002; Mahadev et al., 2007; Piao et al., 2007). As expected, the *sla1Δ* single mutant and the *sla1Δ lsb3Δ ysc84Δ* triple mutant were completely defective in Wsc1-GFP internalization, regardless of HU presence (Figures 7E and 7F; Feliciano and Di Pietro, 2012; Piao et al., 2007). In contrast, *ecm25Δ*, *lsb3Δ*, or *ysc84Δ* single mutants showed little or no defect in CME of Wsc1-GFP in the presence or absence of HU (Figures 7E and 7F). Similarly, internalization of Chs3, the catalytic subunit of chitin synthase-III that is normally removed from the PM through CME (Chuang and Schekman, 1996; Reyes et al., 2007), was not affected by the deletion of *ECM25* (Figure S7). Cdc42 is also considered an endocytic cargo (Ayscough et al., 1999; Irazoqui et al., 2005; Jose et al., 2013; Marco et al., 2007; Orlando et al., 2011), but its intensity and activity at the PM were unchanged in *ecm25Δ* cells (Figures S4C–4E). These data indicate that Ecm25 plays no apparent role in CME, at least with regard to three morphogenesis-related cargoes (Wsc1, Chs3, and Cdc42).

Because Sla1, Lsb3, and Ysc84 interact with Ecm25, we also examined their roles in HU-induced cell elongation. Strikingly, *sla1Δ* cells, despite their major defects in both modes of endocytosis, showed a milder defect in HU-induced cell elongation than *ecm25Δ* cells (Figures 7G and 7H). *ysc84Δ* and *lsb3Δ* cells displayed even milder phenotypes than *sla1Δ* cells (Figures 7G and 7H). However, the *sla1Δ lsb3Δ ysc84Δ* triple mutant showed a similar defect in HU-induced cell elongation as *ecm25Δ* cells (Figures 7G and 7H). This could be caused by the severe endocytic defect (Figures 7C–7F) or dissociation of Ecm25 from endocytic patches (Figures S5B and S5C) in the triple mutant. These data indicate that the severity of defects in HU-induced cell elongation does not correlate with the severity of defects in endocytic activity.

## DISCUSSION

This study suggests that Ecm25 plays an essential role in HU-induced cell elongation by linking Cdc42 to late-stage endocytic sites. This “linker” function is dispensable for normal bud morphogenesis under standard growth conditions but becomes essential for restricting endocytosis and, consequently, exocytosis (because of exo-endocytic coupling) to the bud tip in HU-treated cells to drive cell elongation. In the absence of Ecm25, endocytosis and exocytosis are depolarized from the bud tip while maintaining the mother-bud polarity in HU-treated cells, resulting in an ovoid or round cell morphology. Ecm25 might also fine-tune assembly or maturation of the endocytic sites, a possibility that requires further investigation.

How does Ecm25-controlled polarization of endocytosis drive cell elongation? There are at least two possible scenarios, both of which involve control of polarized exocytosis by polarized endocytosis, a common but poorly understood problem in all eukaryotes (Battey et al., 1999; Gao et al., 2003; Grebnev et al., 2017; Gundelfinger et al., 2003; Johansen et al., 2016; Jose et al., 2013; Marco et al., 2007; Wu et al., 2014). First, experimental and modeling studies indicate that polarized endocytosis could locally recycle polarity regulators such as Cdc42 and Rho1 as well as exocytic components such as vesicle-soluble NSF (N-ethylmaleimide-sensitive factor) attachment protein receptor (v-SNARE) to enable sustained polarized exocytosis to drive cell elongation in budding yeast (Ayscough et al., 1999; Irazoqui et al., 2005; Jose et al., 2013; Marco et al., 2007; Orlando et al., 2011) as well as in filamentous fungi (Caballero-Lima et al., 2013; Hernández-González et al., 2018; Hervás-Aguilar and Peñalva, 2010; Knafler et al., 2019; Shaw et al., 2011). In the absence of polarized endocytosis, such as in HU-treated *ecm25Δ* cells, exocytic components and polarity regulators diffuse on the bud membrane, leading to isotropic growth of the bud and a round cell morphology. Alternatively, depolarized actin patches in HU-treated *ecm25Δ* cells could recruit and locally activate Cdc42 via the patch components Ent1 and Ent2, a pair of functionally redundant yeast epsins that are known to interact with and inhibit Cdc42-GAPs (Aguilar et al., 2006). The actin patch-associated Cdc42, whose local concentration may not be high enough to be detected by fluorescence microscopy, will then direct exocytosis toward that patch. This would also result in depolarized exocytosis in the bud, leading to a round cell morphology. In either scenario, simply changing the location of endocytosis would lead to a change in the location of exocytosis, causing a profound change in cell shape. However, this requires polarization control of endocytosis independent of exocytosis. This possibility is supported by the previous observation that polarized exocytosis is disrupted within 1 min after conditionally inactivating tropomyosin in budding yeast, whereas actin patches remain polarized for more than 15 min in the same cells (Pruyne et al., 1998). Although we cannot rule out involvement of Ecm25 in exocytosis, the fact that Ecm25 associates with late-stage endocytic sites and interacts with multiple endocytic proteins suggests that Ecm25 more likely plays a direct role in endocytosis, which affects cell shape via exo-endocytic coupling.

Cell elongation can be induced by a variety of environmental signals and is apparently a part of the strategy for better survival under stressed conditions. Diploid cells undergo pseudohyphal growth under nitrogen starvation (Gimeno et al., 1992). Haploid cells undergo

filamentous growth in response to short-chain alcohols, mating pheromones, and HU (Dickinson, 1996; Erdman and Snyder, 2001; Jiang and Kang, 2003; Lorenz et al., 2000). These stress-induced cell morphologies share two salient features: cell chain formation (cells are connected via the cell wall after cytokinesis) and cell elongation, both of which would allow the cell to forage for food over a distance under stress conditions (Dickinson, 1996; Erdman and Snyder, 2001; Gimeno et al., 1992; Jiang and Kang, 2003; Lorenz et al., 2000). Genetic evidence indicates that Ecm25 is required for all of these forms of filamentous growth except the one triggered by mating pheromones, in which *ecm25Δ* was not examined (Kang and Jiang, 2005). We show here that Ecm25 is also required for filamentous growth of cells deleted for the septin subunit Shs1 or the DNA damage checkpoint and DNA replication checkpoint kinase Rad53. These observations strongly suggest that Ecm25 is an essential component of a core machinery required for all modes of filamentous cell growth.

Other organisms and cell types also display protrusive cell growth or elongated cell morphology in response to different environmental signals. For example, the opportunistic human fungal pathogen *Candida albicans* can grow as yeast, pseudohyphae, or true hyphae depending on temperature, pH, and serum (Berman, 2006). HU treatment or depletion of the Polo kinase CaCdc5 causes filamentous growth in *Candida* under the yeast growth conditions (Bachewich et al., 2005). In response to chemical signals, vertebrate cells undergo directed cell migration during development (Clay and Halloran, 2013), and tumor cells can undergo metastasis (Lua and Low, 2004). All of these processes involve a dramatic cell shape change; i.e., cell elongation. There are no *bona fide* orthologs of Ecm25 in other fungi and mammalian cells, except *Ashbya gossypii*, a filamentous fungus closely related to *S. cerevisiae*. However, some Ecm25 domains are conserved in mammalian proteins, such as Arhgap1/Cdc42GAP/p50RhoGAP and BPGAP1, both of which contain a Sec14/BCH (BNIP-2 and Cdc42GAP Homology) domain, a proline-rich region, and a RhoGAP domain arranged from the N terminus to the C terminus (Gupta et al., 2012). Both proteins are also involved in receptor-mediated endocytosis and directed cell migration (Clay and Halloran, 2013; Sirokmány et al., 2006). Whether Arhgap1 and BPGAP1 function in these processes in a similar way as Ecm25 does in budding yeast requires further investigation.

## STAR★METHODS

### RESOURCE AVAILABILITY

**Lead contact—**Further information and requests for research materials may be directed to and will be fulfilled by the lead contact, Erfei Bi (ebi@pennmedicine.upenn.edu).

**Materials availability—**Reagents generated in this study will be made available on request.

**Data and code availability—**Data supporting the findings of this study are available within the paper and its supplemental information files and from the authors upon request.

## EXPERIMENTAL MODEL AND SUBJECT DETAILS

Our experimental models are the budding yeast *Saccharomyces cerevisiae*, the fission yeast *Schizosaccharomyces pombe*, and the mammalian cell line HeLa-Kyoto. All the budding strains used in this study are listed in Table S1, and the fission yeast strain and HeLa cells are listed in the Key Resources Table. For culturing the budding yeast cells, standard culture media were used (Guthrie and Fink, 1991). Cells were grown in YPD or synthetic complete (SC) media with specific amino acid(s) dropped out. In some experiments, indicated concentrations hydroxyurea (usually 100 mM) (Sigma-Aldrich, St. Louis, MO) or Latrunculin A (LatA) (usually 200 μM) (Wako Pure Chemicals, Japan) were added to the culture media. All the budding yeast strains were grown at 25°C, unless otherwise indicated. The fission yeast cells were cultured in EMM (Edinburgh Minimal Medium) medium (Mitchison, 1970) and thiamine was added to the culture medium to repress the *Pnmt1* promoter. The HeLa-Kyoto cells stably expressing histone H2B-mCherry (Schmitz et al., 2010) were cultured in Dulbecco's Modified Eagle Medium (DMEM) (ThermoFisher Scientific) containing 5% or 10% fetal bovine serum (FBS) (Invitrogen/GIBCO) at 37°C in the presence of 5% $CO_2$.

## METHOD DETAILS

**Constructions of plasmids and strains—**The pUG36 (*URA3*, *CEN*, *yEGFP3*)-derived plasmids containing different fragments of *ECM25* were constructed by PCR-amplifying the full-length or different fragments of *ECM25* from the genomic DNA isolated from the wild-type strain BY4741 using indicated pairs of primers (Table S2) and then gap-repairing into EcoRI-digested pUG36. Plasmids expressing maltose-binding-protein (MBP)-fusion proteins of Ecm25 fragments, including pMAL-C2-Ecm25-full length (1–599aa), pMAL-C2-Ecm25-N-term+RhoGAP (1–360aa), pMAL-C2-Ecm25-N-term (1–189aa), pMAL-C2-Ecm25-RhoGAP (190–360aa), pMAL-C2-Ecm25-C-term (361–599aa), pMAL-C2-Ecm25 (536–588aa), pMAL-C2-Ecm25 (361–535aa), pMAL-C2-Ecm25 (536–599aa), pMAL-C2-Ecm25 (361–535aa)(PXXP) mutants, were constructed by cloning a BamHI and *Hind*III (both sites introduced in PCR primers)-digested *ECM25* fragment into the corresponding sites of pMAL-C2 (New England BioLabs, Ipswich, MA). DNA fragments encoding Sla1(1–420aa), Sla1(1–420aa, W41S), Sla1(1–420aa, W108S), Lsb3, and Ysc84 were PCR-amplified, digested with BamHI and *Xho*I (sites introduced in the primers), and then cloned into the corresponding sites of pGEX-4X-1 (Sigma) to generate plasmids expressing glutathione-S-transferase (GST)-fusion proteins. The correctness of all the newly constructed plasmids was confirmed by sequencing. Plasmid pMAL-C2-Gic2 (Tcheperegine et al., 2005) and plasmids pGEX-Cdc42, pGEX-Cdc42 (Q61L), and pGEX-Cdc42 (T17N) (Tong et al., 2007) were described previously. PCR-based tagging [with GFP or RFP (mCherry or tagRed)] or deletion of a specific gene in yeast was performed following a standard protocol (Longtine et al., 1998). For constructing strains expressing specific fragments of Ecm25 from its native promoter at the endogenous locus, different alleles of *ECM25* were used to replace the *URA3-KanMX6* cassette inserted in the placement of the *ECM25 ORF*, as described previously (Fang et al., 2010). For the constructions of strains expressing fluorescence-labeled tubulin or Sec4, a pair of primers internal to the open reading frame (ORF) of *TUB1* or *SEC4* (Table S2) was used to amply the entire plasmid

pHIS3p:mRuby2-Tub1+3′UTR::HIS3 (Markus et al., 2015), pASF125 (*pHIS3:GFP-TUB1*, integrative, *URA3*) (Straight et al., 1997), or YIp211-GFP-SEC4 (integrative, *URA3*) as a linear product, which was then transformed into a yeast strain and integrated at the endogenous locus. For the constructions of strains carrying the Cdc42-GTP biosensor, a pair of primer (Table S2) was used to amply a fragment from the plasmid YIp211-GIC2PBD(W23A)-ymNeonGreen (Integrative, *URA3*), which was then integrated at the *URA3* locus of the BY strains (the *ura3* allele in BY4741 was determine by sequencing and the location of the biosensor integration was designed accordingly).

The plasmid pDUAL-GFP-ECM25-xACT(aa536–588) was constructed by PCR-amplifying the fragment carrying *GFP-ECM25-xACT* from the plasmid pUG36-GFP-ECM25-xACT(aa536–588) using the pair of primers listed in Table S2. The DNA fragment was then digested with NheI and AcsI and subcloned into the corresponding sites in pDUAL (Matsuyama et al., 2004). Plasmid pDUAL-GFP-ECM25-xACT, in which GFP-ECM25-xACT is under the control of the thiamine repressible promoter Pnmt1, was digested with NotI, and then transformed into fission yeast cells. The linearized plasmid was expected to integrate at the chromosomal $leu1^{+}$ locus via homologous recombination (Matsuyama et al., 2004), yielding the strain PT4374.

The plasmid pCMV-GFP-puglinker-ECM25-xACT(536–588) was constructed by PCR-amplifying the fragment carrying *puglinker-GFP-ECM25-xACT* from the plasmid pUG36-GFP-ECM25-xACT(aa536–588) using the pair of primers listed in Table S2. The DNA fragment was then inserted into HindIII and SpeI-digested plasmid pCMV-GFP-NMHCII-A (Addgene) using the Quick-Fusion Cloning Kit (BiMake), resulting in the desired plasmid.

**Bimolecular fluorescence complementation (BiFC) assay—**Yeast strains used for the BiFC assay were constructed by a PCR-based approach (Sung and Huh, 2007). A PCR fragment containing the N-terminal fragment of Venus (VN) and *KanMX6* was directly inserted in-frame with the last codon of the desired fragment at the *ECM25* locus in BY4741 (MAT**a**) using different pairs of primers (Table S2), which led to the generation of strains YEF7981 (ECM25-full length-VN- KanMX6), YEF7982 (ECM25-Nterm+RhoGAP-VN-KanMX6), YEF8032 (ECM25-Nterm -VN- KanMX6). Similarly, a PCR fragment containing the N-terminal fragment of Venus (VN) and *KanMX6* was used to replace the stop codon of the *ecm25* alleles in YEF8487 and YEF8483 to generate strains YEF8036 (ECM25-RhoGAP-VN- KanMX6) and YEF8037 (ECM25-Cterm-VN- KanMX6). A PCR fragment containing the *HIS3MX6::pCET1* promoter and the C-terminal fragment of Venus (VC) was directly inserted in-frame before the START codon of *CDC42* at its chromosomal locus in BY4742 (MATα), generating strain YEF7983 (*His3MX6-pCET1-VC*-CDC42). These strains of opposite mating types were mated pairwise and were selected on SC-His plus G418 plates to generate the diploids, which were imaged using the Nikon spinning-disk confocal imaging system as described below.

***In vitro* protein-binding assays—**The pMAL-C2- and pGEX-4X-based plasmids were transformed into *E. coli* strain BL21 (Invitrogen, Carlsbad, CA) to express MBP and GST fusion proteins, respectively. The purification procedure was described before (Fang et al., 2010; Tcheperegine et al., 2005), with some modifications. Briefly, cells were shaken in 250

mL LB plus 100 μg/mL ampicillin at 37°C to $OD_{600}$ about 1.0, and 1 mM IPTG was then added to induce the expression of the fusion proteins at 24°C for 3 h. Cells were collected by centrifugation (6,000rpm, 10min at 4°C), washed twice with ice-cold water, and then resuspended into 5 mL cell lysis buffer (CLB) [the CLB for MBP-tagged proteins: 20 mM Tris-HCl, pH 8.0, 100 mM NaCl, 5mM $MgCl_2$, 0.1% NP-40 and 2 × complete protein inhibitor cocktail tablets (EDTA free) (Roche Diagnostics Co.); the CLB for GST tagged protein: 1 × PBS, 0.1% NP-40, and 2 × complete protein inhibitor cocktail (EDTA free) (Roche Diagnostics Co.)]. Protein extracts were obtained by sonicating cells for 7 × 15 s with a 15 s interval in between on ice, and then centrifuged at 18,500 rpm at 4°C for 20 min.

To purify MBP- or GST-fusion proteins, protein extracts were incubated with prewashed amylose beads (New England Biolabs, Inc.), or glutathione Sepharose 4B beads (GE Healthcare), respectively, and then rocked at 4°C for 1 h. Beads were then washed 5 times each with 1.0 mL corresponding CLB buffer (1 × complete protein inhibitor cocktail tablets). GST-tagged proteins (bound on beads) were resuspended in 1.0 mL CLB. The MBP-tagged proteins were eluted with 300 μL MBP elution buffer (MBP CLB with 0.01M maltose, without the protease inhibitors) by rocking the tube for 10 min at 4°C each time. After four times of elution, all the supernatants were combined into one clean 1.5 mL tube. The concentrations of the purified recombinant proteins were estimated by comparing the sample proteins to bovine serum albumin (BSA) of known concentrations using SDS-PAGE analysis, followed by gel staining with SimplyBlue™ Safe Stain (Invitrogen). For Ecm25 and Cdc42 binding assays, 15 μg MBP-tagged Ecm25 proteins were mixed with 15 μg GST-tagged Cdc42 proteins in 1.5 mL tubes. For Ecm25-patch component (Sla1, Lsb3, and ysc84) binding assays, 5 μg MBP-tagged Ecm25 proteins were mixed with 10 μg GST-tagged patch components in 1.5 mL tubes. The MBP elution buffer was added to the reaction to make a final volume of 400 μL. The binding reaction was incubated with rotation at 4°C for 1 h, and then spun down (3000 rpm for 1min) to pellet the beads, which were then washed 5 times each with 500 μL CLB for MBP-tagged proteins (with 1 × complete protein inhibitor cocktail) at 4°C. The final protein complexes were dissolved in 60 μl 2 × SDS sample buffer, boiled for 5 min, and then resolved by SDS-PAGE, followed by western blotting using mouse monoclonal anti-MBP (Sigma) and mouse monoclonal anti-GST (Abcam, Cambridge, MA) antibodies. A Fast Western Blot Kit (Supersignal West Pico, Mouse, Thermo Scientific) was used for western blotting assay following the manufacturer's instructions.

**F-Actin-binding assay—**The actin-binding capacities of different Ecm25 fragments were determined using the commercially available Actin Binding Protein Spin-Down Assay Biochem Kit (non-muscle actin) (Cytoskeleton, Inc., Denver, CO) (Figures 5A and 5C). The assay was performed following the manufacturer's instructions. This assay involves incubating F-actin and the test protein and then pellets the actin filaments by differential sedimentation. If the test protein could bind F-actin, it would co-pellet with the actin filaments. The MBP elution buffer in which the purified MBP-Ecm25 fragments were dissolved was eliminated by centrifugation using the ultrafiltration tubes, and the recombinant proteins were then dissolved in the actin compatible buffer (containing 50 mM KCl, 20 mM $MgCl_2$). According to the manufacturer's protocol, the test proteins (20 μM)

were incubated in the presence or absence of F-actin at room temperature for 30 min. The reactions were then centrifuged at 150,000 × g at 24°C for 1.5 h to separate the pellet and supernatant. Equal volumes of the supernatant and pellet for each reaction were analyzed by SDS-PAGE, followed by gel staining with SimplyBlue™ Safe Stain (Invitrogen). Stained gels were imaged using a Gel Doc system (Bio-Rad, USA).

**F-actin staining and Latrunculin A (LatA) treatment—**For phalloidin staining of actin filaments, exponentially growing cells (OD600 ~0.3–1.2) were fixed in 3.7% formaldehyde, with shaking at 25°C for 1 h, and then spun down to a pellet size about 10 μL. The pellet was washed three times with PBS (1.0 mL each time), and the cells were then permeabilized in PBS containing 0.2% Triton X-100 for 15 min, and then washed twice with PBS. Cells were then incubated with shaking in 100 μL of PBS buffer containing Alexa Fluor 568-phalloidin (20 U/mL) and BSA (10 mg/mL) at 25°C for 30 min. Cells were washed three times with PBS containing BSA (10 mg/mL), and then resuspended in 10 – 20 μL mounting medium for visualization (Figure 5B).

For testing localization dependency on F-actin, cells were grown to exponential phase and then treated with either 1% DMSO (control) or 100 μM LatA for 20 min (see Figure S5F for the strain carrying *ECM25-GFP*) before documentation by fluorescence microscopy.

For imaging the fission yeast cells (Figure 5D), the strain PT4374 was first cultured in the rich medium YE5S for 6 hours and then switched to EMM (Edinburgh Minimal Medium) medium (Mitchison, 1970) without thiamine overnight (~12 hours) at 25°C to reach $OD_{595}$ value of 0.4–0.6. Two aliquots of the culture were then treated with 200 μM LatA or 1% DMSO as control for 15 min. Samples were fixed in 3.7% formaldehyde for 1 hour and then spun down to pellet cells. The cell pellets were washed three times with PBS, then permeabilized in PBS containing 0.2% Triton X-100 for 15 min and then washed twice again with PBS. The samples were incubated in 100 μL of PBS buffer containing Alexa Fluor 568-phalloidin (20 U/mL) and BSA (10 mg/mL) at 25°C for 60 min. The samples were then washed three times with PBS containing BSA (10 mg/mL), and then resuspended in 10 μL mounting medium for visualization. The imaging conditions were the same as those described for the budding yeast above, except that z stacks were taken at 11 × 1 μm.

For imaging the HeLa-Kyoto cells (Figure 5E), the plasmid pCMV-GFP-puglinker-ECM25-xACT was transfected into HeLa-Kyoto cells using Lipofectamine 2000 (ThermoFisher Scientific) following manufacturer's instructions. The cells were grown in DMEM medium containing 10% FBS in a 12-well dish with a round ploy-D-lysine coated coverglass at bottom at 37°C in the presence of 5% CO2. 48 hours after transfection, cells were treated with 10 μM LatA or 0.05% DMSO as control for 30 min. These cells were fixed in 4% paraformaldehyde in PBS for 10 min and then washed 3 times in PBS. After blocking in PBS with 1% BSA for 20 min, cells were then incubated in 100 μL of PBS buffer containing Alexa Fluor 568-phalloidin (5 U/mL) and 1% BSA at 25°C for 20 min. The cells were washed in PBS for 3 times, then mounting medium was applied before imaging. Photos were taken using the same imaging system as described for the budding yeast, except that z stacks were taken at 11 × 1 μm.

**Endocytosis assays—**All cells were grown in SC media to exponential phase ($OD_{600}$ ~0.2–0.5) at 24°C in the presence or absence of HU (100 mM) for 13 h. For checking fluid-phase endocytosis, Lucifer Yellow (LY) accumulation in the vacuole was assayed as described by previously (Wiederkehr et al., 2001). The cells were concentrated to 2 – 5 $OD_{600}$ U/mL in 1.5 mL tubes. The cell suspension (100 μL) was incubated in the presence of 5 mg/ml LY at 24°C for 2 h. Cells were then washed three times in wash buffer (PBS containing 10 mM sodium azide and 50 mM sodium fluoride), followed by observation by fluorescence microcopy (excitation 450 – 490 nm; emission > 520 nm). The number of cells containing LY-stained or -non-stained vacuoles was counted and calculated in percentage (Figures 7C and 7D). For checking clathrin-mediated endocytosis, the localization patterns of the well characterized transmembrane cargo, Wsc1-GFP (Feliciano and Di Pietro, 2012), in WT, *ecm25Δ*, and other endocytic mutants were determined and the percentages of cells displaying the localization at the PM, the bud cortex, or the endosomes were calculated for each strain under each condition (Figures 7E and 7F).

**Imaging and data analysis—**For the time-lapse experiments throughout this study, the nucleo-cytoplasmic localization of Whi5, an inhibitor of G1/S transcription (Costanzo et al., 2004; de Bruin et al., 2004; Di Talia et al., 2007), and/or the spindle morphology were used as "clocks" to indicate cell cycle stages. Except where noted, cells were grown in SC medium to exponential phase at 25°C in the presence or absence of 100 mM HU for 6 h before imaging. Other imaging experiments were performed as described previously (Oh et al., 2017; Wloka et al., 2013). Cells were spotted onto a poly-lysine-coated glass-bottom dish, and then embedded with SC-containing agarose. SC or SC + HU (100 mM) medium was added to dish for live imaging. Images were acquired using a Nikon microscope (model Eclipse Ti-U, Tokyo, Japan) equipped with a Nikon 100x/1.49NA oil objective (model CFI Apo TIRF 100x), and a Yokogawa spinning-disk confocal scanner unit (model CSU-X1, Tokyo, Japan). A Photometrics QuantEM EMCCD camera (model 512SC, Tucson, AZ, USA) was used for image capture. Solid-state lasers for excitation (488 nm for GFP and 561 nm for RFP) were housed in a launch constructed by Spectral Applied Research (model ILE-400, Richmond Hill, Ontario, Canada). The imaging system was controlled by MetaMorph version 7.8.10.0 (Molecular Devices, Downingtown, PA, USA). Images were taken with z stacks ranging from 8 3 1 μm, 10 × 1 μm or 8 × 1.2 μm for all the experiments, except the one for measuring the lifespan of the Ecm25-GFP/Abp1-RFP patches (Figures 3B–3G and S3A–3L). A sum projection was created with NIH ImageJ (1.51j). For quantification of the fluorescence intensity of Gic2-GFP signal (Figures S4C and S4D), the density around the cell membrane region was calculated by subtracting the fluorescence intensity in background area from the total intensity in an ImageJ-drawn polygon covering the cell membrane region. The data was further calculated as intensity per unit area. Data analyses were performed with Microsoft Excel.

## QUANTIFICATION AND STATISTICAL ANALYSIS

Independent-samples t test was performed using the software SPSS 18.0 (SPSS Inc., Chicago, IL, USA). The data were presented as the mean value ± standard deviation (SD). *P*-values are described in the figure legends or text.

## Supplementary Material

Refer to Web version on PubMed Central for supplementary material.

## ACKNOWLEDGMENTS

We thank Daniel Lew and Andrew Goryachev for critically reading the manuscript; the members of the Bi laboratory, especially Joseph Marquardt, for helpful discussions; Andrea Stout of the CDB Imaging Core for assistance; and Phong Tran, Michael Lampson, Andrew Dancis, Wei Guo, Shaoxiao Wang, Wei-Lih Lee, Chris Burd, and Johannes H. Hegemann for providing plasmids, yeast strains, and mammalian cells. This work was supported by National Institutes of Health grant GM116876 (to E.B.), a fellowship from the China Scholarship Council (to X.D.), National Key R&D Program of China 2018YFD0900400 (to L.F.), National Natural Science Foundation of China 31772866 (to X.-Q.Z.), and the Deutsche Forschungsgesellschaft (DFG) through grants JO 187/8-1 and JO187/5-2 (to N.J.).

## REFERENCES

Adams AEM, Johnson DI, Longnecker RM, Sloat BF, and Pringle JR (1990). *CDC42* and *CDC43*, two additional genes involved in budding and the establishment of cell polarity in the yeast *Saccharomyces cerevisiae*. J. Cell Biol 111, 131–142. [PubMed: 2195038]

Aguilar RC, Longhi SA, Shaw JD, Yeh LY, Kim S, Schön A, Freire E, Hsu A, McCormick WK, Watson HA, and Wendland B (2006). Epsin N-terminal homology domains perform an essential function regulating Cdc42 through binding Cdc42 GTPase-activating proteins. Proc. Natl. Acad. Sci. USA 103, 4116–4121. [PubMed: 16537494]

Ahmadian MR, Stege P, Scheffzek K, and Wittinghofer A (1997). Confirmation of the arginine-finger hypothesis for the GAP-stimulated GTP-hydrolysis reaction of Ras. Nat. Struct. Biol 4, 686–689. [PubMed: 9302992]

Amin E, Jaiswal M, Derewenda U, Reis K, Nouri K, Koessmeier KT, Aspenström P, Somlyo AV, Dvorsky R, and Ahmadian MR (2016). Deciphering the Molecular and Functional Basis of RHOGAP Family Proteins: A SYSTEMATIC APPROACH TOWARD SELECTIVE INACTIVATION OF RHO FAMILY PROTEINS. J. Biol. Chem 291, 20353–20371. [PubMed: 27481945]

Ayscough KR, Stryker J, Pokala N, Sanders M, Crews P, and Drubin DG (1997). High rates of actin filament turnover in budding yeast and roles for actin in establishment and maintenance of cell polarity revealed using the actin inhibitor latrunculin-A. J. Cell Biol 137, 399–416. [PubMed: 9128251]

Ayscough KR, Eby JJ, Lila T, Dewar H, Kozminski KG, and Drubin DG (1999). Sla1p is a functionally modular component of the yeast cortical actin cytoskeleton required for correct localization of both Rho1p-GTPase and Sla2p, a protein with talin homology. Mol. Biol. Cell 10, 1061–1075. [PubMed: 10198057]

Bachewich C, Nantel A, and Whiteway M (2005). Cell cycle arrest during S or M phase generates polarized growth via distinct signals in *Candida albican*s. Mol. Microbiol 57, 942–959. [PubMed: 16091036]

Battey NH, James NC, Greenland AJ, and Brownlee C (1999). Exocytosis and endocytosis. Plant Cell 11, 643–660. [PubMed: 10213784]

Berman J (2006). Morphogenesis and cell cycle progression in *Candida albicans*. Curr. Opin. Microbiol 9, 595–601. [PubMed: 17055773]

Bi E, and Park HO (2012). Cell polarization and cytokinesis in budding yeast. Genetics 191, 347–387. [PubMed: 22701052]

Bi E, and Pringle JR (1996). *ZDS1* and *ZDS2*, genes whose products may regulate Cdc42p in *Saccharomyces cerevisiae*. Mol. Cell. Biol 16, 5264–5275. [PubMed: 8816439]

Boyd C, Hughes T, Pypaert M, and Novick P (2004). Vesicles carry most exocyst subunits to exocytic sites marked by the remaining two subunits, Sec3p and Exo70p. J. Cell Biol 167, 889–901. [PubMed: 15583031]

Brachmann CB, Davies A, Cost GJ, Caputo E, Li J, Hieter P, and Boeke JD (1998). Designer deletion strains derived from *Saccharomyces cerevisiae* S288C: a useful set of strains and plasmids for PCR-mediated gene disruption and other applications. Yeast 14, 115–132. [PubMed: 9483801]

Brown JL, Jaquenoud M, Gulli MP, Chant J, and Peter M (1997). Novel Cdc42-binding proteins Gic1 and Gic2 control cell polarity in yeast. Genes Dev. 11, 2972–2982. [PubMed: 9367980]

Caballero-Lima D, Kaneva IN, Watton SP, Sudbery PE, and Craven CJ (2013). The spatial distribution of the exocyst and actin cortical patches is sufficient to organize hyphal tip growth. Eukaryot. Cell 12, 998–1008. [PubMed: 23666623]

Cai G, and Cresti M (2009). Organelle motility in the pollen tube: a tale of 20 years. J. Exp. Bot 60, 495–508. [PubMed: 19112169]

Carroll CW, Altman R, Schieltz D, Yates JR, and Kellogg D (1998). The septins are required for the mitosis-specific activation of the Gin4 kinase. J. Cell Biol 143, 709–717. [PubMed: 9813092]

Carroll SY, Stimpson HE, Weinberg J, Toret CP, Sun Y, and Drubin DG (2012). Analysis of yeast endocytic site formation and maturation through a regulatory transition point. Mol. Biol. Cell 23, 657–668. [PubMed: 22190733]

Chen G-C, Kim Y-J, and Chan CSM (1997). The Cdc42 GTPase-associated proteins Gic1 and Gic2 are required for polarized cell growth in *Saccharomyces cerevisiae*. Genes Dev. 11, 2958–2971. [PubMed: 9367979]

Chuang JS, and Schekman RW (1996). Differential trafficking and timed localization of two chitin synthase proteins, Chs2p and Chs3p. J. Cell Biol 135, 597–610. [PubMed: 8909536]

Clay MR, and Halloran MC (2013). Rho activation is apically restricted by Arhgap1 in neural crest cells and drives epithelial-to-mesenchymal transition. Development 140, 3198–3209. [PubMed: 23804498]

Costanzo M, Nishikawa JL, Tang X, Millman JS, Schub O, Breitkreuz K, Dewar D, Rupes I, Andrews B, and Tyers M (2004). CDK activity antagonizes Whi5, an inhibitor of G1/S transcription in yeast. Cell 117, 899–913. [PubMed: 15210111]

de Bruin RA, McDonald WH, Kalashnikova TI, Yates J 3rd, and Wittenberg C (2004). Cln3 activates G1-specific transcription via phosphorylation of the SBF bound repressor Whi5. Cell 117, 887–898. [PubMed: 15210110]

Dewar H, Warren DT, Gardiner FC, Gourlay CG, Satish N, Richardson MR, Andrews PD, and Ayscough KR (2002). Novel proteins linking the actin cytoskeleton to the endocytic machinery in *Saccharomyces cerevisiae*. Mol. Biol. Cell 13, 3646–3661. [PubMed: 12388763]

Di Talia S, Skotheim JM, Bean JM, Siggia ED, and Cross FR (2007). The effects of molecular noise and size control on variability in the budding yeast cell cycle. Nature 448, 947–951. [PubMed: 17713537]

Dickinson JR (1996). 'Fusel' alcohols induce hyphal-like extensions and pseudohyphal formation in yeasts. Microbiology (Reading) 142, 1391–1397. [PubMed: 8704979]

Drees BL, Sundin B, Brazeau E, Caviston JP, Chen G-C, Guo W, Kozminski KG, Lau MW, Moskow JJ, Tong A, et al. (2001). A protein interaction map for cell polarity development. J. Cell Biol 154, 549–571. [PubMed: 11489916]

Egelhofer TA, Villén J, McCusker D, Gygi SP, and Kellogg DR (2008). The septins function in G1 pathways that influence the pattern of cell growth in budding yeast. PLoS ONE 3, e2022. [PubMed: 18431499]

Enserink JM, Smolka MB, Zhou H, and Kolodner RD (2006). Checkpoint proteins control morphogenetic events during DNA replication stress in *Saccharomyces cerevisiae*. J. Cell Biol 175, 729–741. [PubMed: 17130284]

Erdman S, and Snyder M (2001). A filamentous growth response mediated by the yeast mating pathway. Genetics 159, 919–928. [PubMed: 11729141]

Fang X, Luo J, Nishihama R, Wloka C, Dravis C, Travaglia M, Iwase M, Vallen EA, and Bi E (2010). Biphasic targeting and cleavage furrow ingression directed by the tail of a myosin II. J. Cell Biol 191, 1333–1350. [PubMed: 21173112]

Feliciano D, and Di Pietro SM (2012). SLAC, a complex between Sla1 and Las17, regulates actin polymerization during clathrin-mediated endocytosis. Mol. Biol. Cell 23, 4256–4272. [PubMed: 22973053]

Feller SM, Ren R, Hanafusa H, and Baltimore D (1994). SH2 and SH3 domains as molecular adhesives: the interactions of Crk and Abl. Trends Biochem. Sci 19, 453–458. [PubMed: 7855886]

Gallego O, Betts MJ, Gvozdenovic-Jeremic J, Maeda K, Matetzki C, Aguilar-Gurrieri C, Beltran-Alvarez P, Bonn S, Fernández-Tornero C, Jensen LJ, et al. (2010). A systematic screen for protein-lipid interactions in *Saccharomyces cerevisiae*. Mol. Syst. Biol 6, 430. [PubMed: 21119626]

Gao XD, Albert S, Tcheperegine SE, Burd CG, Gallwitz D, and Bi E (2003). The GAP activity of Msb3p and Msb4p for the Rab GTPase Sec4p is required for efficient exocytosis and actin organization. J. Cell Biol 162, 635–646. [PubMed: 12913108]

Gavin AC, Aloy P, Grandi P, Krause R, Boesche M, Marzioch M, Rau C, Jensen LJ, Bastuck S, Dümpelfeld B, et al. (2006). Proteome survey reveals modularity of the yeast cell machinery. Nature 440, 631–636. [PubMed: 16429126]

Gimeno CJ, Ljungdahl PO, Styles CA, and Fink GR (1992). Unipolar cell divisions in the yeast *S. cerevisiae* lead to filamentous growth: regulation by starvation and *RAS*. Cell 68, 1077–1090. [PubMed: 1547504]

Gladfelter AS, Bose I, Zyla TR, Bardes ESG, and Lew DJ (2002). Septin ring assembly involves cycles of GTP loading and hydrolysis by Cdc42p. J. Cell Biol 156, 315–326. [PubMed: 11807094]

Goode BL, Eskin JA, and Wendland B (2015). Actin and endocytosis in budding yeast. Genetics 199, 315–358. [PubMed: 25657349]

Gourlay CW, Dewar H, Warren DT, Costa R, Satish N, and Ayscough KR (2003). An interaction between Sla1p and Sla2p plays a role in regulating actin dynamics and endocytosis in budding yeast. J. Cell Sci 116, 2551–2564. [PubMed: 12734398]

Grebnev G, Ntefidou M, and Kost B (2017). Secretion and endocytosis in pollen tubes: models of tip growth in the spot light. Front. Plant Sci 8, 154. [PubMed: 28224002]

Gundelfinger ED, Kessels MM, and Qualmann B (2003). Temporal and spatial coordination of exocytosis and endocytosis. Nat. Rev. Mol. Cell Biol 4, 127–139. [PubMed: 12563290]

Guo W, Grant A, and Novick P (1999a). Exo84p is an exocyst protein essential for secretion. J. Biol. Chem 274, 23558–23564. [PubMed: 10438536]

Guo W, Roth D, Walch-Solimena C, and Novick P (1999b). The exocyst is an effector for Sec4p, targeting secretory vesicles to sites of exocytosis. EMBO J. 18, 1071–1080. [PubMed: 10022848]

Gupta AB, Wee LE, Zhou YT, Hortsch M, and Low BC (2012). Cross-species analyses identify the BNIP-2 and Cdc42GAP homology (BCH) domain as a distinct functional subclass of the CRAL_TRIO/Sec14 superfamily. PLoS ONE 7, e33863. [PubMed: 22479462]

Guthrie C, and Fink GR (1991). Guide to Yeast Genetics and Molecular Biology, First Edition (Academic Press).

Hernández-González M, Bravo-Plaza I, Pinar M, de Los Ríos V, Arst HN Jr., and Peñalva MA (2018). Endocytic recycling via the TGN underlies the polarized hyphal mode of life. PLoS Genet. 14, e1007291. [PubMed: 29608571]

Hervás-Aguilar A, and Peñalva MA (2010). Endocytic machinery protein SlaB is dispensable for polarity establishment but necessary for polarity maintenance in hyphal tip cells of Aspergillus nidulans. Eukaryot. Cell 9, 1504–1518. [PubMed: 20693304]

Howard JP, Hutton JL, Olson JM, and Payne GS (2002). Sla1p serves as the targeting signal recognition factor for NPFX(1,2)D-mediated endocytosis. J. Cell Biol 157, 315–326. [PubMed: 11940605]

Hu CD, Chinenov Y, and Kerppola TK (2002). Visualization of interactions among bZIP and Rel family proteins in living cells using bimolecular fluorescence complementation. Mol. Cell 9, 789–798. [PubMed: 11983170]

Irazoqui JE, Howell AS, Theesfeld CL, and Lew DJ (2005). Opposing roles for actin in Cdc42p polarization. Mol. Biol. Cell 16, 1296–1304. [PubMed: 15616194]

Jiang YW, and Kang CM (2003). Induction of *S. cerevisiae* filamentous differentiation by slowed DNA synthesis involves Mec1, Rad53 and Swe1 checkpoint proteins. Mol. Biol. Cell 14, 5116–5124. [PubMed: 14565980]

Johansen J, Alfaro G, and Beh CT (2016). Polarized exocytosis induces compensatory endocytosis by Sec4p-regulated cortical actin polymerization. PLoS Biol. 14, e1002534. [PubMed: 27526190]

Johnson JL, Erickson JW, and Cerione RA (2009). New insights into how the Rho guanine nucleotide dissociation inhibitor regulates the interaction of Cdc42 with membranes. J. Biol. Chem 284, 23860–23871. [PubMed: 19581296]

Jose M, Tollis S, Nair D, Sibarita JB, and McCusker D (2013). Robust polarity establishment occurs via an endocytosis-based cortical corralling mechanism. J. Cell Biol 200, 407–418. [PubMed: 23401000]

Kaksonen M, Sun Y, and Drubin DG (2003). A pathway for association of receptors, adaptors, and actin during endocytic internalization. Cell 115, 475–487. [PubMed: 14622601]

Kaksonen M, Toret CP, and Drubin DG (2005). A modular design for the clathrin- and actin-mediated endocytosis machinery. Cell 123, 305–320. [PubMed: 16239147]

Kang CM, and Jiang YW (2005). Genome-wide survey of non-essential genes required for slowed DNA synthesis-induced filamentous growth in yeast. Yeast 22, 79–90. [PubMed: 15645503]

Keaton MA, and Lew DJ (2006). Eavesdropping on the cytoskeleton: progress and controversy in the yeast morphogenesis checkpoint. Curr. Opin. Microbiol 9, 540–546. [PubMed: 17055334]

Knafler HC, Smaczynska-de Rooij II, Walker LA, Lee KK, Gow NAR, and Ayscough KR (2019). AP-2-dependent endocytic recycling of the chitin synthase Chs3 regulates polarized growth in *Candida albicans*. MBio 10, 10.

Kubala MH, Kovtun O, Alexandrov K, and Collins BM (2010). Structural and thermodynamic analysis of the GFP:GFP-nanobody complex. Protein Sci. 19, 2389–2401. [PubMed: 20945358]

Lew DJ, and Reed SI (1993). Morphogenesis in the yeast cell cycle: regulation by Cdc28 and cyclins. J. Cell Biol 120, 1305–1320. [PubMed: 8449978]

Li R, Zhang B, and Zheng Y (1997). Structural determinants required for the interaction between Rho GTPase and the GTPase-activating domain of p190. J. Biol. Chem 272, 32830–32835. [PubMed: 9407060]

Logan MR, Jones L, Forsberg D, Bodman A, Baier A, and Eitzen G (2011). Functional analysis of RhoGDI inhibitory activity on vacuole membrane fusion. Biochem. J 434, 445–457. [PubMed: 21171963]

Longtine MS, McKenzie A 3rd, Demarini DJ, Shah NG, Wach A, Brachat A, Philippsen P, and Pringle JR (1998). Additional modules for versatile and economical PCR-based gene deletion and modification in *Saccharomyces cerevisiae*. Yeast 14, 953–961. [PubMed: 9717241]

Lorenz MC, Cutler NS, and Heitman J (2000). Characterization of alcohol-induced filamentous growth in *Saccharomyces cerevisiae*. Mol. Biol. Cell 11, 183–199. [PubMed: 10637301]

Lua BL, and Low BC (2004). BPGAP1 interacts with cortactin and facilitates its translocation to cell periphery for enhanced cell migration. Mol. Biol. Cell 15, 2873–2883. [PubMed: 15064355]

Lussier M, White AM, Sheraton J, di Paolo T, Treadwell J, Southard SB, Horenstein CI, Chen-Weiner J, Ram AF, Kapteyn JC, et al. (1997). Large scale identification of genes involved in cell surface biosynthesis and architecture in *Saccharomyces cerevisiae*. Genetics 147, 435–450. [PubMed: 9335584]

Mack D, Nishimura K, Dennehey BK, Arbogast T, Parkinson J, Toh-e A, Pringle JR, Bender A, and Matsui Y (1996). Identification of the bud emergence gene *BEM4* and its interactions with rho-type GTPases in *Saccharomyces cerevisiae*. Mol. Cell. Biol 16, 4387–4395. [PubMed: 8754839]

Madania A, Dumoulin P, Grava S, Kitamoto H, Schärer-Brodbeck C, Soulard A, Moreau V, and Winsor B (1999). The *Saccharomyces cerevisiae* homologue of human Wiskott-Aldrich syndrome protein Las17p interacts with the Arp2/3 complex. Mol. Biol. Cell 10, 3521–3538. [PubMed: 10512884]

Mahadev RK, Di Pietro SM, Olson JM, Piao HL, Payne GS, and Overduin M (2007). Structure of Sla1p homology domain 1 and interaction with the NPFxD endocytic internalization motif. EMBO J. 26, 1963–1971. [PubMed: 17363896]

Manders EMM, Verbeek FJ, and Aten JA (1993). Measurement of co-localization of objects in dual-color confocal images. J. Microsc 169, 375–382. [PubMed: 33930978]

Marco E, Wedlich-Soldner R, Li R, Altschuler SJ, and Wu LF (2007). Endocytosis optimizes the dynamic localization of membrane proteins that regulate cortical polarity. Cell 129, 411–422. [PubMed: 17448998]

Markus SM, Omer S, Baranowski K, and Lee WL (2015). Improved plasmids for fluorescent protein tagging of microtubules in *Saccharomyces cerevisiae*. Traffic 16, 773–786. [PubMed: 25711127]

Matsuyama A, Shirai A, Yashiroda Y, Kamata A, Horinouchi S, and Yoshida M (2004). pDUAL, a multipurpose, multicopy vector capable of chromosomal integration in fission yeast. Yeast 21, 1289–1305. [PubMed: 15546162]

Mino A, Tanaka K, Kamei T, Umikawa M, Fujiwara T, and Takai Y (1998). Shs1p: a novel member of septin that interacts with spa2p, involved in polarized growth in *saccharomyces cerevisiae*. Biochem. Biophys. Res. Commun 251, 732–736. [PubMed: 9790978]

Mitchison J (1970). Physiological and cytological methods of *Schizosaccharomyces pombe*. Methods Cell Biol. 4, 131–165.

Nirschl JJ, Ghiretti AE, and Holzbaur ELF (2017). The impact of cytoskeletal organization on the local regulation of neuronal transport. Nat. Rev. Neurosci 18, 585–597. [PubMed: 28855741]

Oh Y, Schreiter JH, Okada H, Wloka C, Okada S, Yan D, Duan X, and Bi E (2017). Hof1 and Chs4 interact via F-BAR domain and Sel1-like repeats to control extracellular matrix deposition during cytokinesis. Curr. Biol 27, 2878–2886.e5. [PubMed: 28918945]

Okada S, Leda M, Hanna J, Savage NS, Bi E, and Goryachev AB (2013). Daughter cell identity emerges from the interplay of Cdc42, septins, and exocytosis. Dev. Cell 26, 148–161. [PubMed: 23906065]

Okada S, Lee ME, Bi E, and Park HO (2017). Probing Cdc42 polarization dynamics in budding yeast using a biosensor. Methods Enzymol. 589, 171–190. [PubMed: 28336063]

Onelli E, Idilli AI, and Moscatelli A (2015). Emerging roles for microtubules in angiosperm pollen tube growth highlight new research cues. Front. Plant Sci 6, 51. [PubMed: 25713579]

Orlando K, Sun X, Zhang J, Lu T, Yokomizo L, Wang P, and Guo W (2011). Exo-endocytic trafficking and the septin-based diffusion barrier are required for the maintenance of Cdc42p polarization during budding yeast asymmetric growth. Mol. Biol. Cell 22, 624–633. [PubMed: 21209323]

Panagabko C, Morley S, Hernandez M, Cassolato P, Gordon H, Parsons R, Manor D, and Atkinson J (2003). Ligand specificity in the CRAL-TRIO protein family. Biochemistry 42, 6467–6474. [PubMed: 12767229]

Pardo B, Crabbé L, and Pasero P (2017). Signaling pathways of replication stress in yeast. FEMS Yeast Res. 17, 17.

Park HO, and Bi E (2007). Central roles of small GTPases in the development of cell polarity in yeast and beyond. Microbiol. Mol. Biol. Rev 71, 48–96. [PubMed: 17347519]

Piao HL, Machado IM, and Payne GS (2007). NPFXD-mediated endocytosis is required for polarity and function of a yeast cell wall stress sensor. Mol. Biol. Cell 18, 57–65. [PubMed: 17065552]

Pitoniak A, Chavel CA, Chow J, Smith J, Camara D, Karunanithi S, Li B, Wolfe KH, and Cullen PJ (2015). Cdc42p-interacting protein Bem4p regulates the filamentous-growth mitogen-activated protein kinase pathway. Mol. Cell. Biol 35, 417–436. [PubMed: 25384973]

Pruyne DW, Schott DH, and Bretscher A (1998). Tropomyosin-containing actin cables direct the Myo2p-dependent polarized delivery of secretory vesicles in budding yeast. J. Cell Biol 143, 1931–1945. [PubMed: 9864365]

Reyes A, Sanz M, Duran A, and Roncero C (2007). Chitin synthase III requires Chs4p-dependent translocation of Chs3p into the plasma membrane. J. Cell Sci 120, 1998–2009. [PubMed: 17519287]

Rittinger K, Walker PA, Eccleston JF, Nurmahomed K, Owen D, Laue E, Gamblin SJ, and Smerdon SJ (1997). Crystal structure of a small G protein in complex with the GTPase-activating protein rhoGAP. Nature 388, 693–697. [PubMed: 9262406]

Robertson AS, Allwood EG, Smith AP, Gardiner FC, Costa R, Winder SJ, and Ayscough KR (2009). The WASP homologue Las17 activates the novel actin-regulatory activity of Ysc84 to promote endocytosis in yeast. Mol. Biol. Cell 20, 1618–1628. [PubMed: 19158382]

Rothbauer U, Zolghadr K, Tillib S, Nowak D, Schermelleh L, Gahl A, Backmann N, Conrath K, Muyldermans S, Cardoso MC, and Leonhardt H (2006). Targeting and tracing antigens in live cells with fluorescent nanobodies. Nat. Methods 3, 887–889. [PubMed: 17060912]

Rua D, Tobe BT, and Kron SJ (2001). Cell cycle control of yeast filamentous growth. Curr. Opin. Microbiol 4, 720–727. [PubMed: 11731325]

Salminen A, and Novick PJ (1987). A ras-like protein is required for a post-Golgi event in yeast secretion. Cell 49, 527–538. [PubMed: 3552249]

Schindelin J, Arganda-Carreras I, Frise E, Kaynig V, Longair M, Pietzsch T, Preibisch S, Rueden C, Saalfeld S, Schmid B, et al. (2012). Fiji: an open-source platform for biological-image analysis. Nat. Methods 9, 676–682. [PubMed: 22743772]

Schmitz MH, Held M, Janssens V, Hutchins JR, Hudecz O, Ivanova E, Goris J, Trinkle-Mulcahy L, Lamond AI, Poser I, et al. (2010). Live-cell imaging RNAi screen identifies PP2A-B55alpha and importin-beta1 as key mitotic exit regulators in human cells. Nat. Cell Biol 12, 886–893. [PubMed: 20711181]

Shaw BD, Chung DW, Wang CL, Quintanilla LA, and Upadhyay S (2011). A role for endocytic recycling in hyphal growth. Fungal Biol. 115, 541–546. [PubMed: 21640317]

Sirokmány G, Szidonya L, Káldi K, Gáborik Z, Ligeti E, and Geiszt M (2006). Sec14 homology domain targets p50RhoGAP to endosomes and provides a link between Rab and Rho GTPases. J. Biol. Chem 281, 6096–6105. [PubMed: 16380373]

Sittewelle M, and Monsoro-Burq AH (2018). AKT signaling displays multi-faceted functions in neural crest development. Dev. Biol 444 (Suppl 1), S144–S155. [PubMed: 29859890]

Sloat BF, Adams A, and Pringle JR (1981). Roles of the *CDC24* gene product in cellular morphogenesis during the *Saccharomyces cerevisiae* cell cycle. J. Cell Biol 89, 395–405. [PubMed: 7019215]

Smolka MB, Chen SH, Maddox PS, Enserink JM, Albuquerque CP, Wei XX, Desai A, Kolodner RD, and Zhou H (2006). An FHA domain-mediated protein interaction network of Rad53 reveals its role in polarized cell growth. J. Cell Biol 175, 743–753. [PubMed: 17130285]

Straight AF, Marshall WF, Sedat JW, and Murray AW (1997). Mitosis in living budding yeast: anaphase A but no metaphase plate. Science 277, 574–578. [PubMed: 9228009]

Sung MK, and Huh WK (2007). Bimolecular fluorescence complementation analysis system for in vivo detection of protein-protein interaction in *Saccharomyces cerevisiae*. Yeast 24, 767–775. [PubMed: 17534848]

Tang HY, Xu J, and Cai M (2000). Pan1p, End3p, and S1a1p, three yeast proteins required for normal cortical actin cytoskeleton organization, associate with each other and play essential roles in cell wall morphogenesis. Mol. Cell. Biol 20, 12–25. [PubMed: 10594004]

Tarassov K, Messier V, Landry CR, Radinovic S, Serna Molina MM, Shames I, Malitskaya Y, Vogel J, Bussey H, and Michnick SW (2008). An in vivo map of the yeast protein interactome. Science 320, 1465–1470. [PubMed: 18467557]

Tcheperegine SE, Gao XD, and Bi E (2005). Regulation of cell polarity by interactions of Msb3 and Msb4 with Cdc42 and polarisome components. Mol. Cell. Biol 25, 8567–8580. [PubMed: 16166638]

Tkach JM, Yimit A, Lee AY, Riffle M, Costanzo M, Jaschob D, Hendry JA, Ou J, Moffat J, Boone C, et al. (2012). Dissecting DNA damage response pathways by analysing protein localization and abundance changes during DNA replication stress. Nat. Cell Biol 14, 966–976. [PubMed: 22842922]

Tolsma TO, Cuevas LM, and Di Pietro SM (2018). The Sla1 adaptor-clathrin interaction regulates coat formation and progression of endocytosis. Traffic 19, 446–462. [PubMed: 29542219]

Tong Z, Gao XD, Howell AS, Bose I, Lew DJ, and Bi E (2007). Adjacent positioning of cellular structures enabled by a Cdc42 GTPase-activating protein-mediated zone of inhibition. J. Cell Biol 179, 1375–1384. [PubMed: 18166650]

Tonikian R, Xin X, Toret CP, Gfeller D, Landgraf C, Panni S, Paoluzi S, Castagnoli L, Currell B, Seshagiri S, et al. (2009). Bayesian modeling of the yeast SH3 domain interactome predicts spatiotemporal dynamics of endocytosis proteins. PLoS Biol. 7, e1000218. [PubMed: 19841731]

Weiss EL (2012). Mitotic exit and separation of mother and daughter cells. Genetics 192, 1165–1202. [PubMed: 23212898]

Wesseling M, Sakkers TR, de Jager SCA, Pasterkamp G, and Goumans MJ (2018). The morphological and molecular mechanisms of epithelial/endothelial-to-mesenchymal transition and its involvement in atherosclerosis. Vascul. Pharmacol 106, 1–8. [PubMed: 29471141]

Wiederkehr A, Meier KD, and Riezman H (2001). Identification and characterization of Saccharomyces cerevisiae mutants defective in fluid-phase endocytosis. Yeast 18, 759–773. [PubMed: 11378903]

Wloka C, Vallen EA, Thé L, Fang X, Oh Y, and Bi E (2013). Immobile myosin-II plays a scaffolding role during cytokinesis in budding yeast. J. Cell Biol 200, 271–286. [PubMed: 23358243]

Wu X, and Jiang YW (2005). Possible integration of upstream signals at Cdc42 in filamentous differentiation of *S. cerevisiae*. Yeast 22, 1069–1077. [PubMed: 16200521]

Wu LG, Hamid E, Shin W, and Chiang HC (2014). Exocytosis and endocytosis: modes, functions, and coupling mechanisms. Annu. Rev. Physiol 76, 301–331. [PubMed: 24274740]

Yang J, McCormick MA, Zheng J, Xie Z, Tsuchiya M, Tsuchiyama S, El-Samad H, Ouyang Q, Kaeberlein M, Kennedy BK, and Li H (2015). Systematic analysis of asymmetric partitioning of yeast proteome between mother and daughter cells reveals “aging factors” and mechanism of lifespan asymmetry. Proc. Natl. Acad. Sci. USA 112, 11977–11982. [PubMed: 26351681]

Young ME, Cooper JA, and Bridgman PC (2004). Yeast actin patches are networks of branched actin filaments. J. Cell Biol 166, 629–635. [PubMed: 15337772]

Zeng J, Feng S, Wu B, and Guo W (2017). Polarized Exocytosis. Cold Spring Harb. Perspect. Biol 9, a027870. [PubMed: 28246185]

Zhang X, Bi E, Novick P, Du L, Kozminski KG, Lipschutz JH, and Guo W (2001). Cdc42 interacts with the exocyst and regulates polarized secretion. J. Biol. Chem 276, 46745–46750. [PubMed: 11595741]

Zheng Y, Cerione R, and Bender A (1994). Control of the yeast bud-site assembly GTPase Cdc42. Catalysis of guanine nucleotide exchange by Cdc24 and stimulation of GTPase activity by Bem3. J. Biol. Chem 269, 2369–2372. [PubMed: 8300560]

Ziman M, Preuss D, Mulholland J, O’Brien JM, Botstein D, and Johnson DI (1993). Subcellular localization of Cdc42p, a *Saccharomyces cerevisiae* GTP-binding protein involved in the control of cell polarity. Mol. Biol. Cell 4, 1307–1316. [PubMed: 8167411]

## Highlights

- Ecm25 is essential for stress-induced cell elongation
- Ecm25 interacts with Cdc42 and multiple endocytic proteins
- Ecm25 contains an actin filament-binding motif
- Ecm25 links Cdc42 to the late-stage endocytic sites during stress response

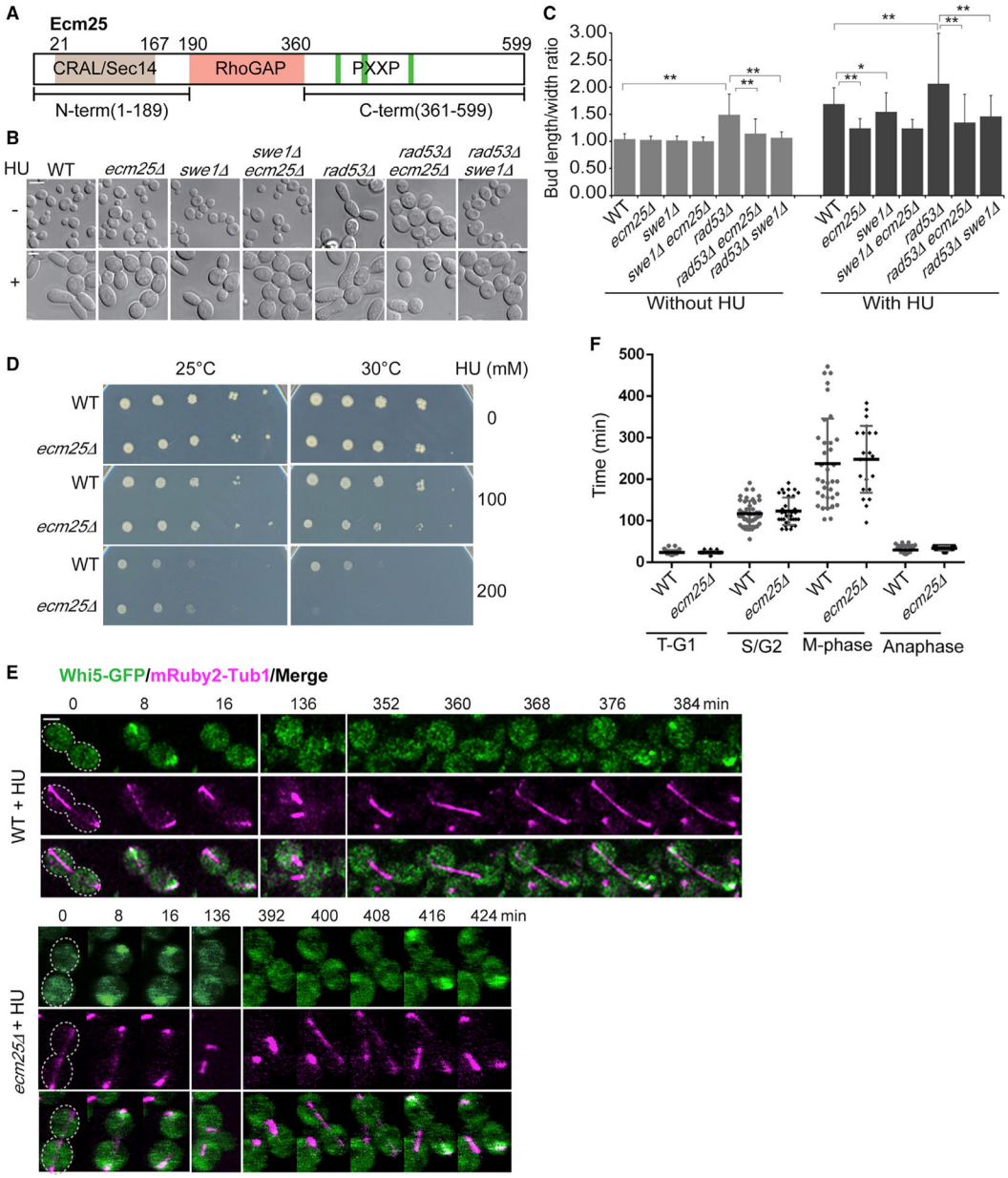


**Figure 1. Ecm25 is essential for stress-induced cell elongation regardless of the cues and cell cycle regulation**

(A) Domains and motifs in Ecm25. CRAL/Sec14, CRAL-TRIO/Sec14 lipid binding domain; RhoGAP, Rho GAP domain; PXXP, PXXP motifs. N-term and C-term, the indicated N- and C-terminal fragments of Ecm25.

(B) Representative cell morphologies of BY-background strains with or without HU treatment (100 mM HU at 25°C for ~13 h). Yeast strains: WT (BY4741), *ecm25Δ* (YEF7957), *swe1Δ* (YEF7958), *ecm25Δ swe1Δ* (YEF7961), *rad53Δ* (YEF8061), *rad53Δ ecm25Δ* (YEF8062), and *rad53Δ swe1Δ* (YEF8490). All experiments were performed at 25°C unless indicated otherwise. Scale bars, 4 μm for −HU and 2 μm for +HU.

(C) Quantitative analysis of the bud length/width ratios for data shown in (B). About 100 cells were analyzed for each strain, and data were expressed as mean value ± standard deviation (SD). **$p < 0.001$, *$p = 0.002$.

(D) *ecm25Δ* cells are sensitive to 200 mM HU at 30°C. Ten-fold serial dilutions of WT (BY4741) and *ecm25Δ* (YEF7956) cultures were spotted on synthetic complete (SC) plates in the presence or absence of HU (100 mM or 200 mM) and incubated at 25°C and 30°C, respectively, for 4 days before documentation.

(E) Time-lapse analysis of cell cycle progression (Whi5-GFP and Tub1-RFP) in HU-treated WT (YEF7942) and *ecm25Δ* (YEF7962) cells in BY-background strains. Selected frames are chosen from time-lapse series taken with an 8-min interval. Scale bar, 4 μm. See also Figures S1B and S1C and Video S1.

(F) Quantitative analysis of cell cycle progression for the data shown in (E). T-G1 (telophase to G1 phase), from appearance to disappearance of Whi5-GFP in the nucleus; S/G2, from disappearance of Whi5-GFP from the nucleus to appearance of a mitotic spindle (Tub1-FRP) of 2 μm in length; M-phase, from appearance of a 2-μm mitotic spindle at the mother side of the bud neck to start of spindle elongation; anaphase, from start of spindle elongation to its maximum length accompanied by appearance of Whi5-GFP in the nucleus. Data are expressed as mean value ± SD.

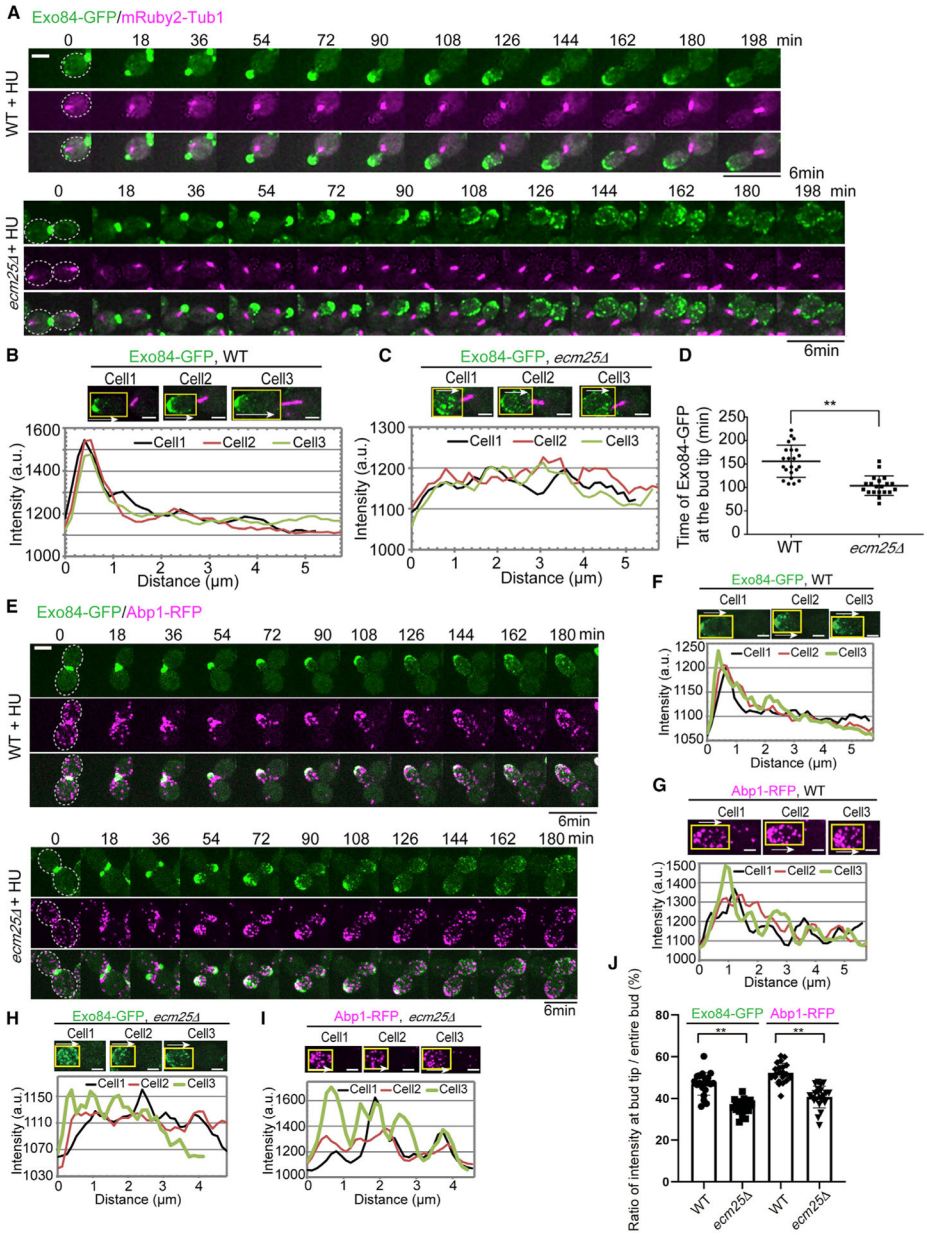


**Figure 2. Ecm25 is required for sustained polarization of exo-endocytosis at the bud tip during stress-induced cell elongation**

(A) Time-lapse analysis of Exo84-GFP localization during the cell cycle (Tub1-RFP) in HU-treated WT (YEF7970) and *ecm25Δ* (YEF8031) cells. Interval, 6 min. Scale bar, 3 μm. See also Figure S2 and Videos S2 and S3.

(B and C) Intensity profile analysis of M-phase Exo84-GFP localization in the daughter compartments of HU-treated WT (YEF7970) (B) and *ecm25Δ* (YEF8031) (C) cells. The distance for the x axis (in micrometers) was measured from the bud tip to the bud neck (white arrow) for the entire daughter compartment (yellow box). Scale bar, 3 μm.

(D) Quantitative analysis of the duration of Exo84-GFP at the bud tip during the cell cycle in HU-treated WT and *ecm25Δ* cells (from the data shown in A). For WT cells, n = 22; for *ecm25Δ* cells, n = 20. Data were expressed as mean value ± SD. **p < 0.001.

(E) Time-lapse analysis of Exo84-GFP and Abp1-RFP localization during the cell cycle in HU-treated WT (YEF7781) and *ecm25Δ* (YEF8217) cells. Interval, 6 min. Scale bar, 3 μm. See also Video S2.

(F–I) Intensity profile analysis of Exo84-GFP and Abp1-RFP localization in the daughter compartments of HU-treated WT (YEF7781) (F and G) and *ecm25Δ* (YEF8217) (H and I) cells 150 min after bud emergence. The distance for the x axis (in micrometers) was measured from the bud tip to the bud neck (white arrow) for the entire daughter compartment (yellow box). Scale bar, 3 μm.

(J) Quantitative analysis of Exo84 and Abp1 polarization at the bud tip during mitosis in HU-treated WT (YEF7781, n = 21) and *ecm25Δ* (strain YEF8217, n = 22) cells. The time-lapse data acquired in (E) were used to determine the polarization index of Exo84-GFP and Abp1-RFP by calculating the ratio of the fluorescence intensity for each protein at the bud tip versus the entire bud during mitosis. The bud tip is defined as the apical region that accounts for 32.19% of the bud area in WT or 32.71% of the bud area in *ecm25Δ* cells. WT cells entered mitosis 136.57 ± 11.05 min after bud emergence, whereas *ecm25Δ* cells entered mitosis 134.73 ± 11.52 min after bud emergence (Figures 2A and 2E). At this point, the ratio of fluorescence intensity for each protein at the defined bud-tip area versus the entire bud was calculated and plotted. Data are expressed as mean value ± SD. **$p < 0.001$.

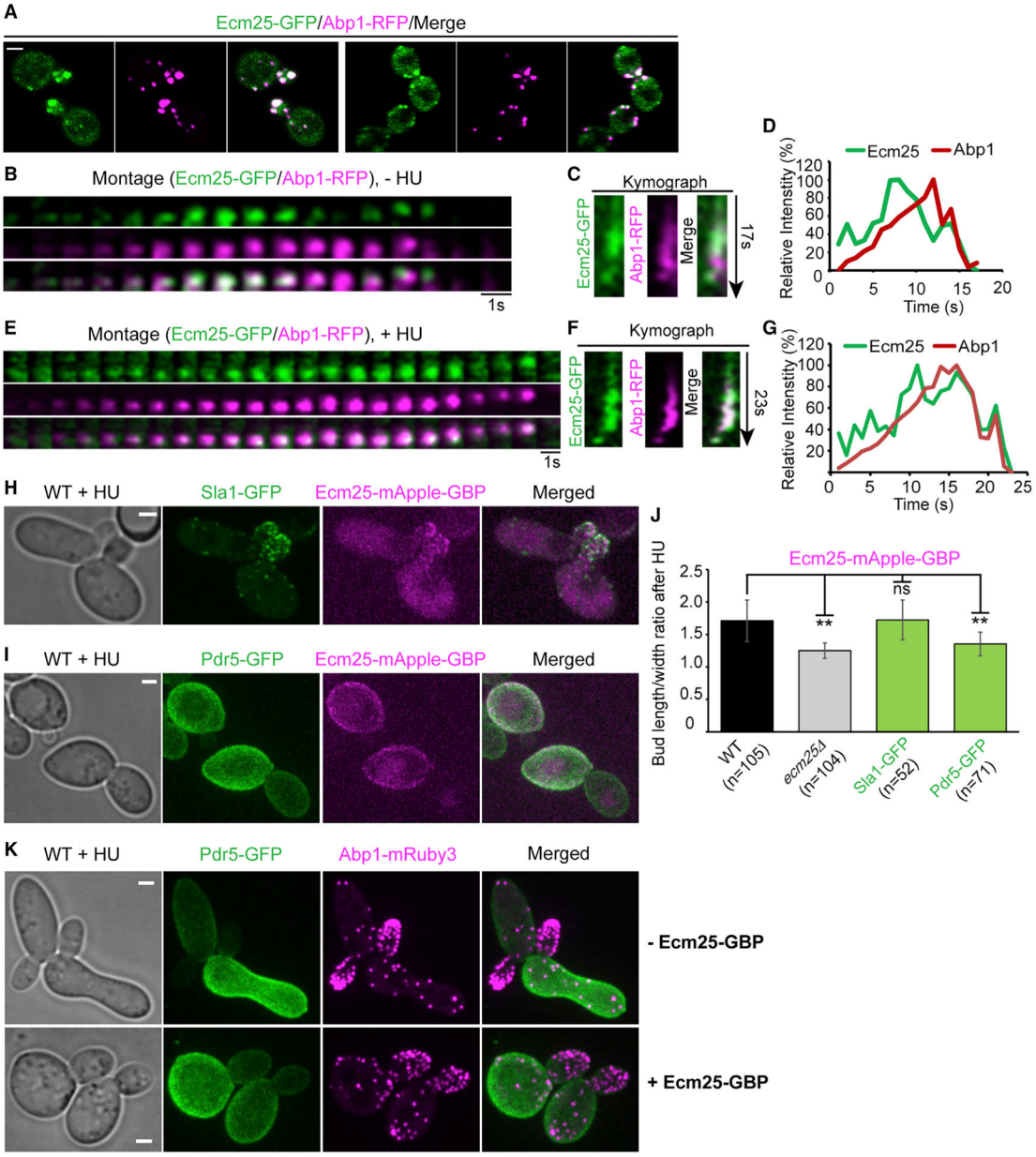


**Figure 3. Association of Ecm25 with the endocytic sites is critical for its role in HU-induced cell elongation**

(A) Spatial relationship between Ecm25-GFP expressed from its native promoter and the endocytic machinery (Abp1-RFP) in small- and large-budded WT cells (YEF7779). Scale bar, 2 μm.

(B–D) Time-lapse analysis of the localization dynamics of Ecm25-GFP and Abp1-RFP at endocytic sites in non-HU-treated WT cells (YEF7779). Single-focal-plane images were acquired at 1-s intervals. A montage (B), kymograph (C), and relative intensity (D) of both proteins for a representative cell are shown. See also Figures S3A–S3F.

(E–G) Time-lapse analysis of the localization dynamics of Ecm25-GFP and Abp1-RFP at endocytic sites in HU-treated WT cells (YEF7779). See also Figures S3G–S3L. (H and I) The effect of targeting Ecm25 to the endocytic site or the PM at the mother side on HU-

induced cell elongation. Cells of strain YEF9781 carrying Sla1-GFP and Ecm25-mApple-GBP (H) and strain YEF9789 carrying Pdr5-GFP and Ecm25-mApple-GBP (I) were grown exponentially in SC medium containing 100 mM HU at 25°C for ~16 h and then harvested for morphological documentation. Some of the Ecm25-mApple-GBP molecules seemed to localize to vacuole-like structures under this condition. Scale bar, 2 μm.

(J) Quantitative analysis of the bud length/width ratios for data shown in (H) and (I). Data are expressed as mean value ± SD. **$p < 0.001$; ns, not significant.

(K) The effect of targeting Ecm25 to the PM at the mother side on endocytic site distribution. Cells of strain YEF9868 carrying Pdr5-GFP and Abp1-mRuby3 (top) and strain YEF9876 carrying Pdr5-GFP, Ecm25-GBP, and Abp1-mRuby3 (bottom) were grown and documented as described for in (H) and (I). Scale bar, 2 μm.

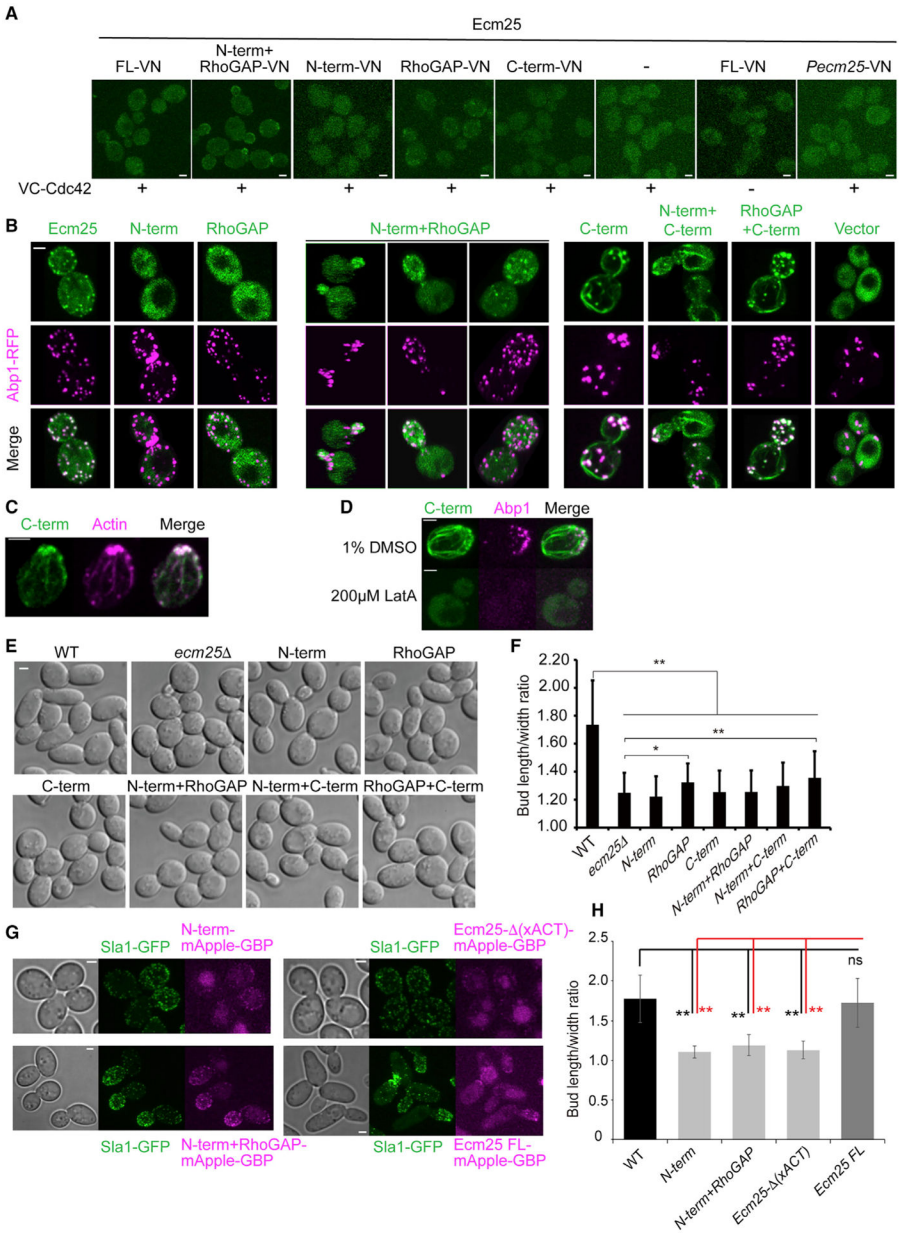


**Figure 4. The N-terminal Sec14-like and RhoGAP domains of Ecm25 mediate its interaction with Cdc42 and are required for stress-induced cell elongation**

(A) BiFC-detected interactions between Cdc42 and FL Ecm25 (YEF7988), its N-term +RhoGAP (YEF7991), N-term (YEF8049), RhoGAP (YEF8316), or C-term (YEF8324) fragment. Negative controls include VC-Cdc42 (YEF10451), Ecm25-full-length (FL)-VN (YEF10450), and *Pecm25*-VN/VC-Cdc42 (YEF10426). VC, the C-terminal fragment of Venus; VN, the N-terminal fragment of Venus. Scale bar, 2 μm. See also Figure S4.

(B) Localization of GFP-tagged FL Ecm25 (YEF7805) and its N-term (YEF7882), RhoGAP (YEF7813), N-term+RhoGAP (YEF7883), C-term (YEF7809), N-term+C-term (YEF7814), and RhoGAP+C-term (YEF7808) fragments expressed from a heterologous promoter on the plasmid vector pUG36 in relation to Abp1-RFP in the absence of HU. Scale bar, 2 μm.

(C) The C-term on Ecm25 associates with both actin patches and actin cables. Cells of strain YEF7809 (*ecm25Δ ABP1-RFP, pUG36-GFP-ECM25-C-term*) were fixed and stained by Alexa Fluor 568 (red)-conjugated phalloidin to visualize filamentous actin cables and patches. Scale bar, 2 μm.

(D) The patch- and cable-like structures formed by GFP-Ecm25-C-term are sensitive to LatA treatment (200 μM LatA for 10 min). Yeast strain: YEF7809 (*ecm25Δ ABP1-RFP, pUG36-GFP-ECM25-C-term*). Scale bar, 2 μm.

(E and F) Differential contributions of different Ecm25 domains to its essential role in HU-induced cell elongation. HU-treated cells of strains expressing FL Ecm25 (BY4741) or its N-term (YEF8482), RhoGAP (YEF8487), C-term (YEF8483), N-term+RhoGAP (YEF8486), N-term+C-term (YEF8485), or RhoGAP+C-term (YEF8484) from its native promoter at the endogenous locus or containing *ecm25Δ* (YEF7956) were documented by differential interference contrast (DIC) microscopy (E) and quantified for the bud length/width ratios (F). Scale bar, 2 μm. Data are expressed as mean value ± SD. $^{**}p < 0.001$, $^{*}p = 0.003$.

(G and H) The effect of targeting different Ecm25 fragments to endocytic sites on HU-induced cell elongation. Cells of the WT strain (BY4741) as well as strains carrying Sla1-GFP and Ecm25-N-term-mApple-GBP (YEF10421) or Ecm25-N-term+RhoGAP-mApple-GBP (YEF10422), Ecm25-Δ(xACT)-mApple-GBP (YEF10423), or Ecm25 FL-mApple-GBP (YEF9781) were grown exponentially in SC medium containing 100 mM HU at 25°C for ~16 h and then harvested for morphological documentation by bright-field and fluorescence microscopy (G). Some of the Ecm25-mApple-GBP molecules, regardless of the truncations, seemed to localize to vacuole-like structures under this condition. Scale bar, 2 μm. Data from (G) were used for the quantitative analysis of the bud length/width ratios (H). Data were expressed as mean value ± SD. $^{**}p < 0.001$; ns, not significant.

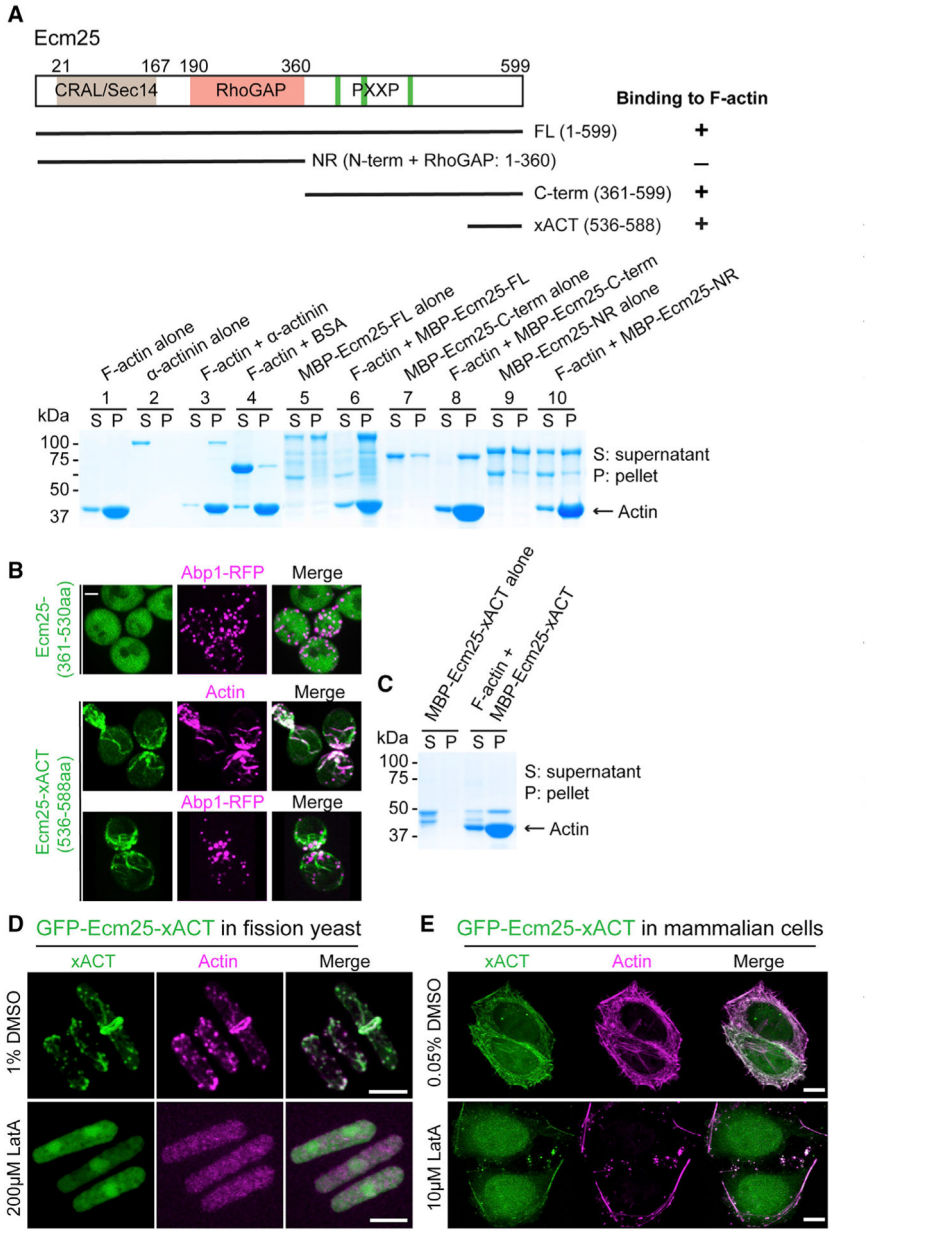


**Figure 5. Ecm25 binds to actin filaments in budding yeast, fission yeast, and mammalian cells via the xACT motif**

(A) Ecm25 binds F-actin via its C terminus (in 3 independent experiments). Top: depiction of the Ecm25 fragments and their binding capacities to F-actin. Bottom: the positive control α-actinin, the negative control BSA, and MBP fusions of the FL and different fragments of Ecm25 were used for the F-actin pelleting assay using the Non-Muscle Actin Binding Protein Spin-Down Biochem Kit.

(B) The xACT motif in the C terminus of Ecm25 localizes mainly to actin cables and occasionally to actin patches. Plasmids pUG36-GFP-Ecm25(361–530aa) and pUG36-GFP-Ecm25-xACT(536–588aa) were transformed into YEF7788 (*ecm25Δ::HIS3 ABP1-tagRED-Kan*) to generate strains YEF7815 and YEF7854, respectively, which were then imaged by spinning-disk confocal microscopy. Cells of YEF7854 were also stained by Alexa Fluor 568

(red)-conjugated phalloidin to visualize co-localization of the Ecm25-xACT fragment and F-actin (center panel). Scale bar, 2 μm.

(C) Ecm25 binds to F-actin via its xACT motif. MBP-Ecm25-xACT(536–588aa) was used in the *in vitro* F-actin-binding assay as described in (A).

(D) Ecm25-xACT expressed in fission yeast labels actin patches, actin cables, and the actin ring. Cells of the fission yeast strain PT4374 expressing GFP-Ecm25-xACT from the thiamine-repressible promoter (Pnmt1; integrated in the chromosome) were grown in Edinburgh minimal medium (EMM) without thiamine at 25°C. Two aliquots of the culture were treated with 1% DMSO (control) and 200 μM LatA, respectively, for 15 min and then stained for F-actin. Scale bar, 5 μm.

(E) Ecm25-xACT expressed in mammalian cells labels actin filaments. HeLa-Kyoto cells expressing GFP-Ecm25-xACT from the pCMV promoter carried on a plasmid were cultured in DMEM and then treated with 0.05% DMSO (control) or 10 μM LatA for 30 min. The treated cells were then stained for F-actin. Scale bar, 10 μm.

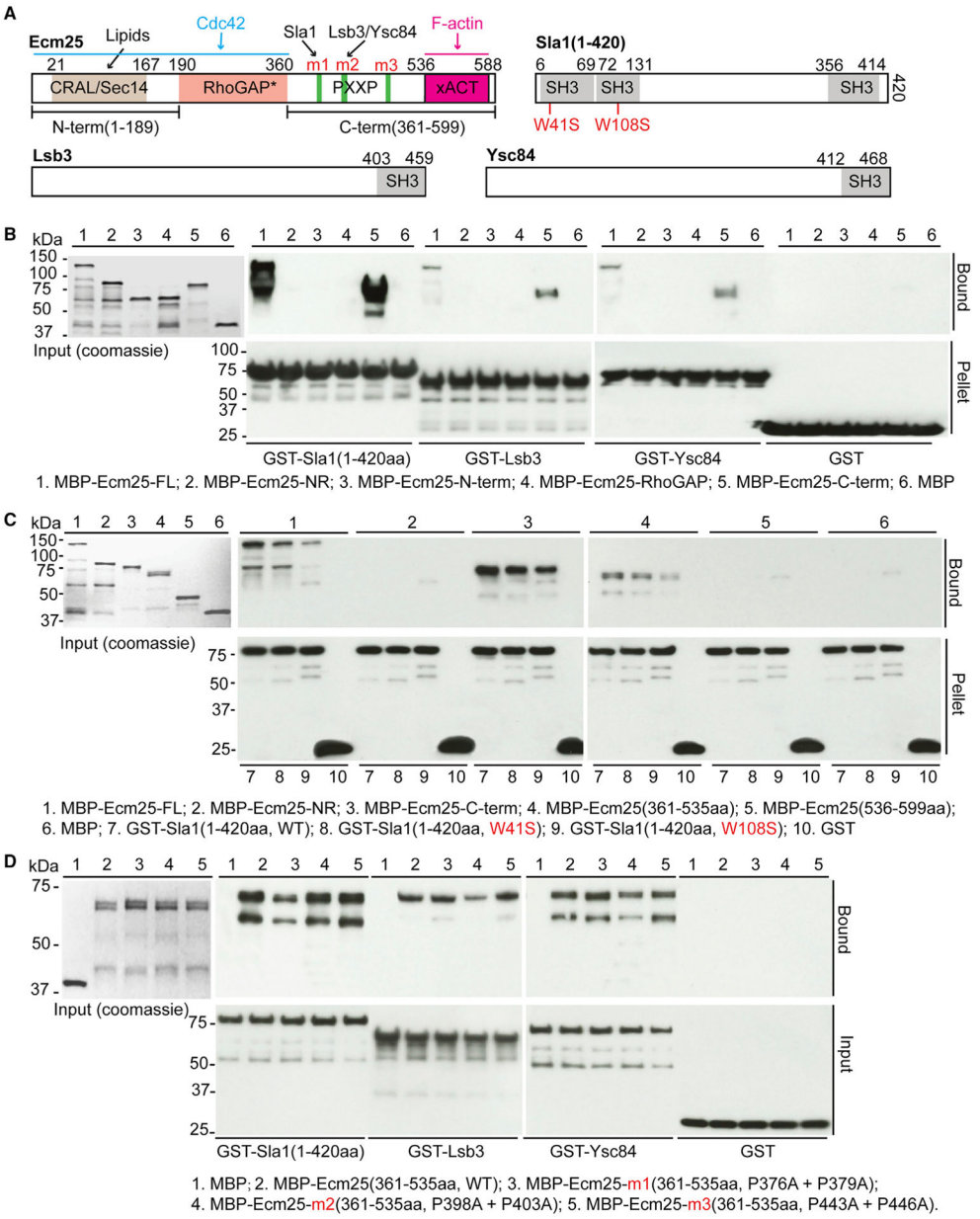


**Figure 6. Ecm25 interacts directly with the actin-patch components Sla1, Lsb3, and Ysc84**

(A) Schematics showing the domains, motifs, and/or binding partners of Ecm25, Sla1(1–420aa), Lsb3, and Ysc84. For Ecm25: CRAL/Sec14, lipid binding domain; RhoGAP*, inactive (marked by an asterisk) Rho GAP domain; m1–m3, mutations introduced at each of the three PXXP motifs; xACT, F-actin-binding motif. For Sla1, Lsb3, and Ysc84: SH3, Src homology-3; W41S and W108S, mutations introduced at the first and second SH3 domains of Sla1, respectively.

(B) Ecm25 interacts with Sla1, Lsb3, and Ysc84 via its C terminus (in 2 independent experiments). MBP fusions of the indicated Ecm25 fragments were examined for interactions with GST fusions of Sla1(1–420aa), Lsb3, and Ysc84 *in vitro* using the GST pull-down assay.

(C) Ecm25 interacts with the first two SH3 domains of Sla1 via a PXXP motif-containing region (in 3 independent experiments). MBP fusions of the indicated Ecm25 fragments were examined for interactions with GST fusions of the WT and SH3-domain variants of Sla1(1–420aa).

(D) Ecm25 interacts with the SH3 domains of Sla1 and the paralogs Lsb3 and Ysc84 via distinct PXXP motifs (in 3 independent experiments). MBP fusions of the WT and PXXP-motif variants (m1, m2, or m3) of the Ecm25(361–535aa) fragment were examined for interactions with GST fusions of Sla1(1–420aa), Lsb3, and Ysc84.

See also Figure S6.

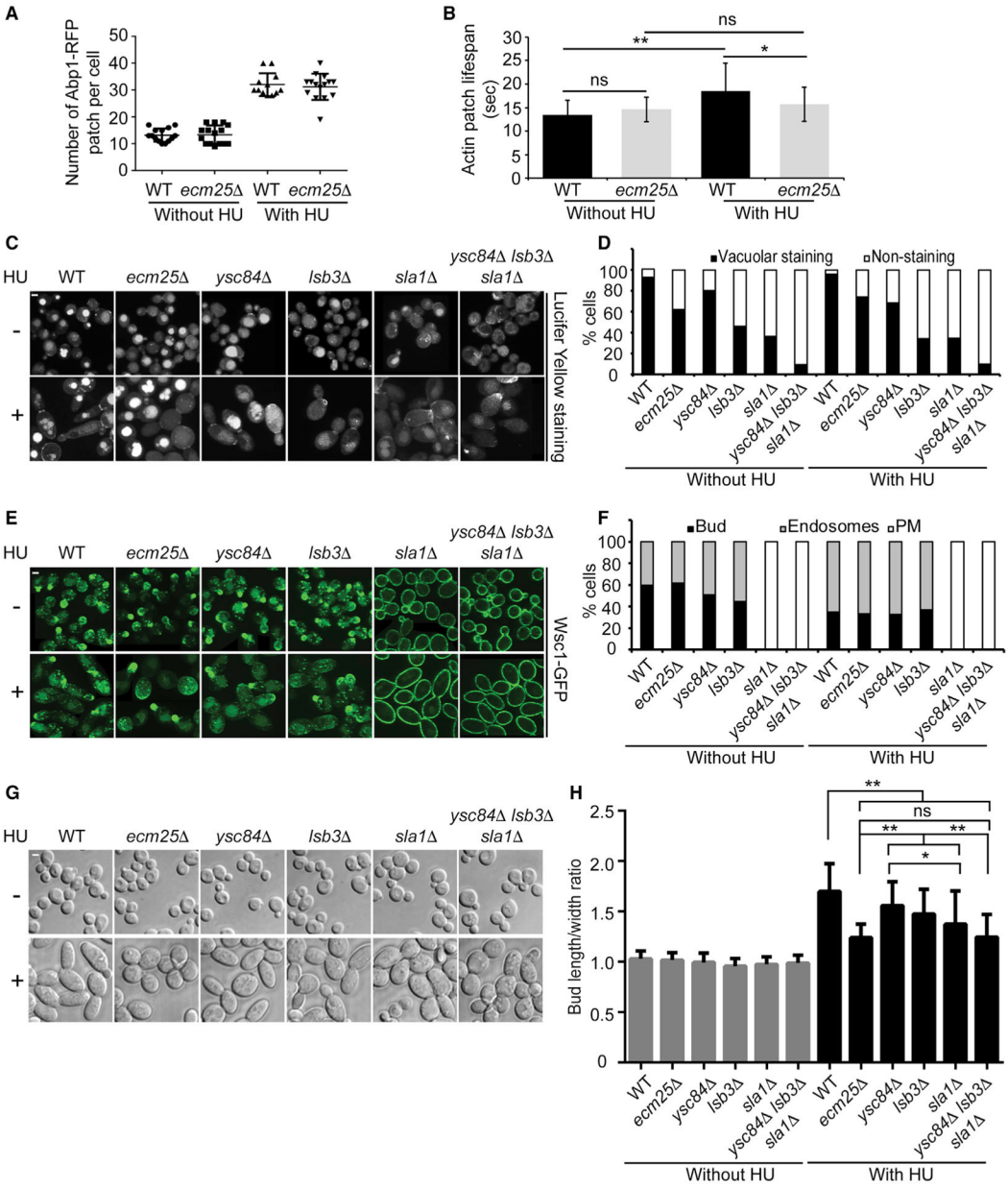


**Figure 7. Ecm25 does not play a major role in fluid-phase endocytosis and CME**

(A) Deletion of *ECM25* does not change the number of actin patches per cell in the presence or absence of HU. WT (YEF7756) and *ecm25Δ* (YEF7788) cells were cultured in SC medium at 25°C in the absence or presence of HU (100 mM for 8 h), and then the number of actin patches in large-budded cells was counted for each strain under each growth condition. Numbers of cells counted: WT without HU, n = 14; *ecm25Δ* without HU, n = 15; WT with HU, n = 12; *ecm25Δ* with HU, n = 15.

(B) Deletion of *ECM25* does not overtly affect actin patch behavior. The growth conditions were the same as described in (A), except that the actin patches were imaged with a 1-s interval. Numbers of patches quantified: WT without HU, n = 23; *ecm25Δ* without HU, n =

25; WT with HU, n = 40; *ecm25Δ* with HU, n = 42. Data are expressed as mean value ± SD. **p = 0.0011, *p = 0.0127.

(C) Deletion of *ECM25* causes only a mild defect in fluid-phase endocytosis. Cells of the indicated strains were grown in the presence or absence of 100 mM HU and then processed for the LY assay. Scale bar, 2 μm.

(D) Quantitative analysis of data from (C). Cell numbers analyzed for each strain and each condition were as follows: WT (BY4741) without HU, n = 116; WT (BY4741) with HU, n = 227; *ecm25Δ* (YEF7956) without HU, n = 170; *ecm25Δ* (YEF7956) with HU, n = 220; *ysc84Δ* (YEF8181) without HU, n = 133; *ysc84Δ* (YEF8181) with HU, n = 172; *lsb3Δ* (YEF8184) without HU, n = 120; *lsb3Δ* (YEF8184) with HU, n = 114; *sla1Δ* (YEF8187) without HU, n = 102; *sla1Δ* (YEF8187) with HU, n = 208; *ysc84Δ lsb3Δ sla1Δ* (YEF8978) without HU, n = 120; *ysc84Δ lsb3Δ sla1Δ* (YEF8978) with HU, n = 186.

(E) Ecm25 plays no apparent role in CME. Cells of the indicated strains were grown in the presence or absence of 100 mM HU and then documented by fluorescence microscopy. Scale bar, 2 μm.

(F) Quantitative analysis of data from (E). Cell numbers analyzed for each strain and each condition were as follows: WT (YEF9049) without HU, n = 129; WT (YEF9049) with HU, n = 150; *ecm25Δ* (YEF9010) without HU, n = 171; *ecm25Δ* (YEF9010) with HU, n = 150; *ysc84Δ* (YEF9050) without HU, n = 136; *ysc84Δ* (YEF9050) with HU, n = 131; *lsb3Δ* (YEF9051) without HU, n = 155; *lsb3Δ* (YEF9051) with HU, n = 135; *sla1Δ* (YEF9052) without HU, n = 147; *sla1Δ* (YEF9052) with HU, n = 136; *ysc84Δ lsb3Δ sla1Δ* (YEF9053) without HU, n = 148; *ysc84Δ lsb3Δ sla1Δ* (YEF9053) with HU, n = 123.

(G) Different actin patch mutants display differential defects in HU-induced cell elongation. Cells of the strains WT (BY4741), *ecm25Δ* (YEF7956), *ysc84Δ* (YEF8181), *lsb3Δ* (YEF8184), *sla1Δ* (YEF8187), and *ysc84Δ lsb3Δ sla1Δ* (YEF8978) were grown in the presence or absence of 100 mM HU at 25°C for ~13 h before morphology documentation by DIC microscopy. Scale bar, 2 μm.

(H) Quantitative analysis of the bud length/width ratios for data shown in (G). Cell numbers analyzed for each strain and each condition were as follows: WT without HU, n = 67; WT with HU, n = 81; *ecm25Δ* without HU, n = 105; *ecm25Δ* with HU, n = 93; *ysc84Δ* without HU, n = 84; *ysc84Δ* with HU, n = 86; *lsb3Δ* without HU, n = 67; *lsb3Δ* with HU, n = 87; *sla1Δ* without HU, n = 80; *sla1Δ* with HU, n = 80; *ysc84Δ lsb3Δ sla1Δ* without HU, n = 91; *ysc84Δ lsb3Δ sla1Δ* with HU, n = 82. Data are expressed as mean value ± SD. **p < 0.001, *p = 0.005.

## KEY RESOURCES TABLE

| REAGENT or RESOURCE | SOURCE | IDENTIFIER |
|---|---|---|
| Antibodies | | |
| Mouse monoclonal anti-MBP (Maltose Binding Protein) | Sigma | Cat #: M1321; RRID: AB_1079301 |
| Mouse monoclonal anti-GST antibody | Abcam | Cat #: ab92; RRID: AB_307067 |
| Mouse monoclonal anti-GFP antibody | Covance | Cat #: MMS-118P; RRID: AB_291290 |
| Bacterial and virus strains | | |
| *E. coli* strain DH5α | Invitrogen | Cat #: 18258012 |
| *E. coli* strain BL21(DE3) | Invitrogen | Cat #: C600003 |
| *E.coli XL1* blue: *recA1 endA1 gyrA96 thi-1 hsdR17 supE44 relA1 lac* | Stratagene | Cat #: 200249 |
| Chemicals, peptides, and recombinant proteins | | |
| Hydroxyurea | Sigma | Cat #: H8627 |
| Latrunculin A | Wako Pure Chemicals | Cat #: 125-04363 |
| Alexa Fluor 568-phalloidin | Invitrogen | Cat #: A12380 |
| Lucifer Yellow CH dilithium salt | Sigma | Cat # L0259 |
| Amylose beads | New England Biolabs, Inc. | Cat #: E8021L |
| Glutathione Sepharose 4B beads | GE Healthcare | Cat #: 17075601 |
| Complete protein inhibitor cocktail tablets (EDTA free) | Roche Diagnostics Co. | Cat #: 11836170001 |
| SimplyBlue™ Safe Stain | Invitrogen | Cat #: LC6060 |
| Restore™ Western Blot Stripping Buffer | Thermo Scientific | Cat #: 21059 |
| Dulbecco's Modified Eagle Medium (DMEM) | ThermoFisher Scientific | Cat# 11965-084 |
| Fetal Bovine Serum (FBS) | Invitrogen/GIBCO | Cat# 16000-044 |
| Lipofectamine 2000 | ThermoFisher Scientific | Cat# 11668027 |
| MBP-Ecm25 fragments [full length, N terminus, N terminus plus RhoGAP, RhoGAP, C terminus, 361-535aa, 536-599aa, 536-588aa, 361-535aa(P376A,P379A), 361-535aa(P398A,P403A), 361-535aa(P443A, P446A)] | This paper | N/A |
| MBP-Gic2, MBP | Tcheperegine et al., 2005 | N/A |
| GST-Cdc42, GST-Cdc42(Q61L), GST-Cdc42(T17N), GST | Tong et al., 2007 | N/A |
| GST-SLA1(1-420aa), GST-LSB3, GST-YSC84, GST-SLA1(1-420aa, W41S), GST-SLA1(1-420aa, W108S) | This paper | N/A |
| Critical commercial assays | | |
| Pierce Fast Western Blot Kits, SuperSignal West Pico, Mouse | Thermo Scientific | Cat # 35060 |
| Actin Binding Protein Biochem Kit (Non-Muscle Actin) | Cytoskeleton, Inc | Cat # BK013 |
| Quick-Fusion Cloning Kit | BiMake | Cat #: B22612 |
| Experimental models: Organisms/strains | | |
| *Saccharomyces cerevisiae* strains, see Table S1 | This paper | N/A |
| *Schizosaccharomyces pombe* strain PT4374, *h-Pnmt1-GFP-ECM25-xACT(aa536-588)::leu1⁺ leu1Δ3′ ura4-D18 ade6-210* | This paper (Phong Tran) | N/A |
| *HeLa-Kyoto cells* stably expressing histone H2B-mCherry | Schmitz et al., 2010 | N/A |
| Oligonucleotides | | |
| Primers, see Table S2 | This paper | N/A |
| Recombinant DNA | | |

| REAGENT or RESOURCE | SOURCE | IDENTIFIER |
|---|---|---|
| Plasmid: pFA6a-HIS3MX6 | Addgene | Cat #: 41596 |
| Plasmid: pFA6a-KanMX6 | Addgene | Cat #: 39296 |
| DNA: ABP1-tagRED-Kan | This paper | YEF6367 |
| Plasmid: pFA6a-URA3-KanMX6 (cassette) | Tong et al., 2007 | N/A |
| Plasmid: pUG36 (N-YEGFP3, URA3) | J.H. Hegemann | N/A |
| Plasmid: pFA6a-VN-KanMX6 | Sung and Huh, 2007 | N/A |
| Plasmid: pFA6a-VC-HIS3MX6 | Sung and Huh, 2007 | N/A |
| Plasmid: pHIS3p:mRuby2-Tub1+3 ′UTR::HIS3 | Markus et al., 2015 | N/A |
| Plasmid: pHIS3p:mRuby2-Tub1+3 ′UTR::HPH | Markus et al., 2015 | N/A |
| Plasmid: YIP211-GFP-SEC4-URA3 | This paper | N/A |
| Plasmid: YIp211-GIC2PBD(W23A)-ymNeonGreen-URA3 | This paper | N/A |
| Plasmid: pFA6a-link-yoEGFP-Kan | Addgene | Cat #: 44900 |
| Plasmid: pFA6a-link-yoEGFP-CaURA3 | Addgene | Cat #: 44872 |
| Plasmid: pFA6a-link-yoEGFP-Sp*HIS*5 | Addgene | Cat #: 44836 |
| Plasmid: pFA6a-link-mEGFP-*HphMX*6 | This paper | N/A |
| Plasmid: pFA6a-link-mApple-GBP-CaURA3 | This paper | N/A |
| Plasmid: pFA6a-link-GBP-CaURA3 | This paper | N/A |
| Plasmid: pDUAL | Matsuyama et al., 2004 | N/A |
| Plasmid: pDUAL-GFP-ECM25-xACT(aa536-588) | This paper | N/A |
| Plasmid: pCMV-GFP-NMHC-IIA | Addgene | Cat #: 11347 |
| Plasmid: pCMV-GFP-puglinker-ECM25-xACT(aa536-588) | This paper | N/A |
| Software and algorithms | | |
| MetaMorph version 7.8.10.0 | Molecular Devices | https://www.moleculardevices.com/ |
| Fiji | Schindelin et al.,2012 | https://imagej.net/Fiji |
| NIH ImageJ (1.51j) | NIH | https://imagej.nih.gov/ij/ |
| Prism Version 5 | GraphPad Software | https://www.blueprism.com/ |